Available online at www.sciencedirect.com

ScienceDirect

Geochimica et Cosmochimica Acta 143 (2014) 232–252

Geochimica et Cosmochimica Acta

www.elsevier.com/locate/gca

Isotope evolution in the HIMU reservoir beneath St. Helena: Implications for the mantle recycling of U and Th

Takeshi Hanyu [a,*], Hiroshi Kawabata [b,a], Yoshiyuki Tatsumi [c,a], Jun-Ichi Kimura [a], Hironobu Hyodo [d], Keiko Sato [a,d,e], Takashi Miyazaki [a], Qing Chang [a], Yuka Hirahara [a], Toshiro Takahashi [a,f], Ryoko Senda [a], Shun'ichi Nakai [g]

[a] *Institute for Research on Earth Evolution, Japan Agency for Marine-Earth Science and Technology, Yokosuka 237-0061, Japan*
[b] *Faculty of Earth Science, Department of Natural Science, Kochi University, Kochi 780-8520, Japan*
[c] *Earth and Planetary Sciences, Kobe University, Kobe 657-8501, Japan*
[d] *Research Institute of Natural Sciences, Okayama University of Science, Okayama 700-0005, Japan*
[e] *Submarine Resources Research Project, Japan Agency for Marine-Earth Science and Technology, Yokosuka 237-0061, Japan*
[f] *Department of Geology, Faculty of Science, Niigata University, Niigata 950-2181, Japan*
[g] *Earthquake Research Institute, The University of Tokyo, Bunkyo-ku, Tokyo 113-0032, Japan*

Available online 27 March 2014

Abstract

HIMU (high-μ; $^{238}U/^{204}Pb$) is a mantle reservoir that has been thought to form by subduction and subsequent storage of ancient oceanic crust and lithosphere in the mantle. In order to constrain the processes that acted on subducted materials over several billion years, we present precise Pb–Sr–Nd–Hf–He isotopic data together with $^{40}Ar/^{39}Ar$ and K/Ar ages of HIMU lavas from St. Helena in the Atlantic. Clinopyroxene separates were analyzed together with whole-rock samples to better describe the geochemical characteristics of the HIMU component. Although isotopic variations are small in the St. Helena lavas (20.6–21.0 for $^{206}Pb/^{204}Pb$) between 12 and 8 Ma, the younger lavas have more HIMU-like isotopic compositions than the older lavas. The mixing arrays defined by these lavas are remarkably similar to those observed in HIMU lavas from Austral Islands in the Pacific, suggesting that the two HIMU reservoirs located in different mantle domains are characterized by similar isotopic compositions with radiogenic $^{206}Pb/^{204}Pb$ and $^{208}Pb/^{204}Pb$, enriched Nd and Hf isotopes, depleted Sr isotopes, and radiogenic $^{3}He/^{4}He$. However, there is a significant difference between the St. Helena and Austral Islands lavas in $^{207}Pb/^{204}Pb$. The St. Helena lavas show systematically higher $^{207}Pb/^{204}Pb$ for a given $^{206}Pb/^{204}Pb$. Lead isotope evolution models suggest that both HIMU reservoirs formed around 2 Ga; however, the HIMU reservoir for St. Helena is about 0.3 Ga older than that for Austral Islands. The relation between $^{206}Pb/^{204}Pb$ and $^{208}Pb/^{204}Pb$ could reflect the time-integrated κ ($^{232}Th/^{238}U$) in the components. The HIMU components for St. Helena and Austral Islands have κ values between 3.3 and 3.7, which are intermediate between the present-day fresh mid-ocean ridge basalts (MORB; 2.6–3.2) and the chondritic silicate Earth (~4). This is consistent with the model that the HIMU precursor is subducted oceanic crust created around 2 Ga from depleted upper mantle, in which κ monotonously decreased from the chondritic to the present-day values since late Archean or early Proterozoic, because of enhanced U recycling from the Earth's surface back to the mantle in response to the increasing oxygen levels in the hydrosphere. Moreover, the fact that the HIMU components have much higher κ than the present-day hydrothermally altered MORB (0.2–2) suggests that either the HIMU precursor was an unaltered ancient oceanic crust, or more likely, an altered oceanic crust with minimal U enrichment by hydrothermal fluids in the less oxic marine environment of the late Archean or early Proterozoic. The unradiogenic $^{87}Sr/^{86}Sr$ of the HIMU components also suggests formation of

* Corresponding author. Address: Institute for Research on Earth Evolution, Japan Agency for Marine-Earth Science and Technology, Natsushima-cho 2-15, Yokosuka 237-0061, Japan. Tel.: +81 46 867 9807.
E-mail address: hanyut@jamstec.go.jp (T. Hanyu).

http://dx.doi.org/10.1016/j.gca.2014.03.016

ancient oceanic crust altered with hydrothermal fluids having much lower $^{87}Sr/^{86}Sr$ in that eon than at present, followed by removal of Rb from it by subduction dehydration.

1. INTRODUCTION

Compositional variations in ocean island basalts (OIB) and mid-ocean ridge basalts (MORB) document a geochemically heterogeneous mantle (e.g., Zindler and Hart, 1986; Hofmann, 1997; Stracke, 2012 and references therein). While mantle heterogeneities may be partly ascribed to internal mantle differentiation induced by partial melting and melt transport (Vollmer, 1983; McKenzie, 1989), another important process is the input of surface materials to the Earth's interior via subduction (Hofmann and White, 1982; McKenzie and O'Nions, 1983; Tatsumi, 2005). This idea is based on the geochemical similarities between some OIB sourced from the deep mantle and oceanic crust, continental crust, sediment, and lithospheric mantle (Zindler and Hart, 1986; Weaver, 1991; Hauri and Hart, 1993; Woodhead and Devey, 1993; Eisele et al., 2002; Stracke et al., 2003, 2005; Willbold and Stracke, 2006, 2010; Jackson et al., 2007; Kawabata et al., 2011). However, the geochemical features of OIB cannot be solely explained by recycling of such materials without chemical modification through subduction.

For instance, a group of OIB with extremely radiogenic Pb isotopes, referred to as HIMU (high-μ; $\mu = {}^{238}U/{}^{204}Pb$), require very high U/Pb in their source (Tatsumoto, 1978; Vidal et al., 1984; Palacz and Saunders, 1986; Chauvel et al., 1992). The HIMU lavas also exhibit unique trace element characteristics of depletion in highly incompatible elements (e.g., Cs, Rb, and Ba) and fluid-mobile elements (e.g., K, Pb, and Sr) (Dupuy et al., 1988; Weaver, 1991; Kogiso et al., 1997a; Willbold and Stracke, 2006). Depletion in highly incompatible elements can be explained by the involvement of subducted oceanic crust and lithospheric mantle in their source. On the other hand, depletion in fluid-mobile elements and high-μ require other processes that modified geochemical compositions of subducted oceanic crust. The debate is ongoing regarding the origin of HIMU; remelting of metasomatized lithospheric mantle is a possible model to account for the unique geochemical feature of the HIMU lavas (McKenzie, 1989; Niu and O'Hara, 2003; Pilet et al., 2008), but another viable process that has been often invoked is hydrothermal alteration of oceanic crust and subsequent dehydration of such altered oceanic crust during subduction (Dupuy et al., 1988; Weaver, 1991; Chauvel et al., 1992; Woodhead, 1996; Kogiso et al., 1997a; Stracke et al., 2003, 2005; Willbold and Stracke, 2006; Hanyu et al., 2011a; Kawabata et al., 2011).

The occurrence of oceanic basalts with robust HIMU signatures ($^{206}Pb/^{204}Pb > 20.5$) is limited to St. Helena in the Atlantic and several volcanic islands in the Austral–Cook Islands in the South Pacific (Nakamura and Tatsumoto, 1988; Chaffey et al., 1989; Chauvel et al., 1992; Hémond et al., 1994; Woodhead, 1996; Kogiso et al., 1997b; Schiano et al., 2001; Lassiter et al., 2003; Stracke et al., 2005; Hanyu et al., 2011a). Highly radiogenic Pb isotopic compositions imply >1.5 Ga old origin of their mantle source (Chauvel et al., 1992; Woodhead, 1996; Thirlwall, 1997; Hanyu et al., 2011a). The recent discovery of mass-independent fractionation of sulfur isotopes in the Mangaia HIMU lavas in Austral–Cook Islands suggests the involvement of recycled Archean oceanic crust in their source (Cabral et al., 2013). Some OIB also show similar trace element features but have less radiogenic Pb isotopes (e.g., $^{206}Pb/^{204}Pb < 20.5$) than the lavas from St. Helena and Austral Islands (Vidal, 1992; Thirlwall, 1997; Day et al., 2010). Since these lavas have characteristically low $^{207}Pb/^{204}Pb$ for a given $^{206}Pb/^{204}Pb$, young subducted material (<1.5 Ga) has been suggested as their source component (Vidal, 1992; Thirlwall, 1997). Subducted material with various ages should indeed exist ubiquitously in the mantle (e.g., Christensen and Hofmann, 1994; Stracke et al., 2005; Brandenburg et al., 2008), and it is critical to precisely determine and compare geochemical characteristics of OIB to better understand how the subducted materials were processed and when the geochemical reservoirs formed in the mantle.

In this study, we report new isotopic data and radiometric ages for HIMU lavas from St. Helena, and examine the detailed geochemical characteristics of the HIMU component in conjunction with previously reported major and trace element compositions for the same samples (Kawabata et al., 2011). Note that we use the term "HIMU component" as a hypothetical material with extreme geochemical compositions and the term "HIMU reservoir" as a mantle domain that contains the HIMU component. The HIMU lavas inherit geochemical signatures from the HIMU component, but in many cases such signatures are diluted by components from other sources. Previous studies demonstrated that the HIMU lavas from the Austral Islands display isotopic mixing arrays between the HIMU component and depleted mantle component (Chauvel et al., 1992; Schiano et al., 2001; Lassiter et al., 2003; Hanyu et al., 2011a, 2013). The geochemical data presented here for the St. Helena HIMU lavas also show isotopic mixing arrays and highlight the similarities and differences between the HIMU lavas from St. Helena and Austral Islands. Based on the comparisons, the origin of the two HIMU reservoirs for St. Helena beneath Atlantic and Austral Islands beneath Pacific will be discussed.

2. GEOLOGICAL BACKGROUND

St. Helena is part of a scattered volcanic chain on the slowly (22–31 mm/y) migrating African plate (O'Connor et al., 1999). The ages of the seamounts become progressively older along the volcanic chain to the northeast up to 80–82 Ma (O'Connor and le Roex, 1992). Although the present

position of the active hotspot is not well identified, some seamounts located west of St. Helena exhibit relatively young ages down to 2.6 Ma (O'Connor et al., 1999). Only St. Helena records both submarine and subaerial eruptions in the volcanic chain, forming an ocean island with ~5% of its total volume above sea level (Baker, 1969). Previous reported K/Ar ages of on-land lavas range from 7 to 14 Ma (Abdel-Monem and Gast, 1967; Baker et al., 1967). Chaffey et al. (1989) described subaerial volcanic activity ranging from 7 to 9 Ma based on their preliminary age data. These ages are much younger than the ones predicted according to the hotspot theory because the Bagration Seamount located ~50 km to the northwest was dated at 18–19 Ma. St. Helena could have started its submarine volcanic activity much earlier than the subaerial volcanism (O'Connor et al., 1999).

The subaerial St. Helena volcanics mostly comprise alkaline lava flows, pyroclastic rocks, and dykes (Fig. 1). A NE–SW elongated island was established by the coalescence of two major shield volcanoes; an erosional unconformity separates the older NE volcano from the younger SW volcano. Each volcanic shield is further divided into stratigraphic units based on field observations and radiometric ages (Baker et al., 1967; Baker, 1969). The Lower Shield of the NE volcano is the oldest among the exposed rocks on the island and is of submarine origin. This unit consists of volcaniclastic rocks obscured by numerous basaltic dykes. The volcanic activity shifted from submarine to subaerial after an eruption hiatus, and the NE Main Shield formed on top of the NE Lower Shield by emplacement of lava piles and pyroclastic rocks. The volcanic products of the SW volcano are divided into three major units, which are referred to as Lower, Main, and Upper Shields, separated by erosional unconformities (Baker et al., 1967). The Lower and Main Shields of the SW volcano mainly consist of lava flows and pyroclastic rocks. The Lower Shield is exposed in the southern part of the island where the volcanic edifice is severely eroded, whereas the Main Shield covers the central and western surface of the SW volcano. The lavas of the Upper Shield flooded the flank of the SW volcano to the east and concealed part of the NE volcano beneath them. The final volcanic phase is represented by variously differentiated lavas that intruded the shield volcanoes (Late Intrusives).

Rock samples from the volcanic shield and Late Intrusives exhibit a broad but consecutive compositional trend in terms of major elements (Baker, 1969; Chaffey et al., 1989; Kawabata et al., 2011). The shield-building lavas exhibit various rock types from picro-basalt to trachyte

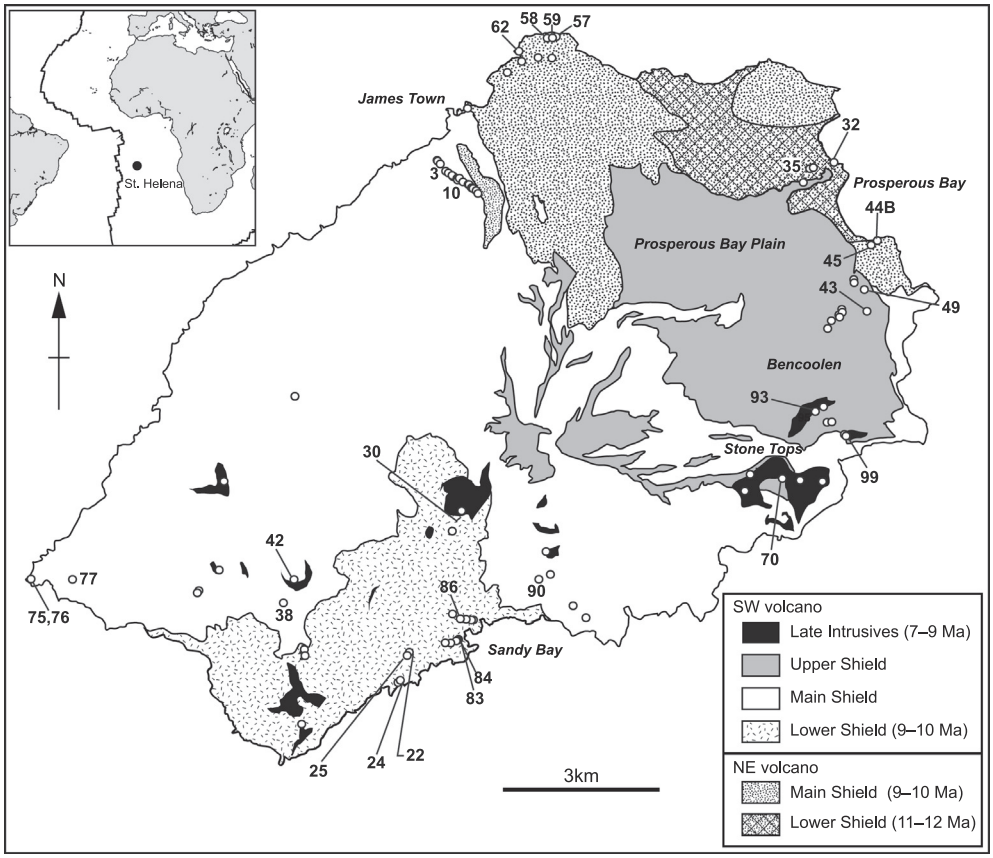

Fig. 1. Geological map of St. Helena. The volcanic units are after Baker (1969). Open circles denote sample localities. Samples used in this study are annotated by sample numbers. The ages of the stratigraphic units are approximately 11–12 Ma for the NE Lower Shield, 9–10 Ma for the NE Main Shield and SW Lower Shield, and 7–9 Ma for the Late Intrusives. The ages of the SW Main and Upper Shields were not constrained but they should be between those of the SW Lower Shield and the Late Intrusives.

with alkali basalts being the most abundant. Rock compositions tend to be more differentiated in the later stage of volcanic activity, and the Late Intrusives are predominantly trachyte and phonolite. There is no systematic difference between the rocks from the NE and SW volcanoes in terms of major and trace element compositions. Some rocks are alkali basalts with coarse (up to 15 mm) olivine and clinopyroxene phenocrysts, referred to as ankaramite. Such rocks are abundant in the early shield phases (Lower and Main Shields of the NE volcano and Lower Shield of the SW volcano). Whole-rock MgO content is positively correlated with the mode of olivine plus clinopyroxene (Kawabata et al., 2011). The variation in major elements is mostly controlled by the fractionation and accumulation of olivine and clinopyroxene phenocrysts, where the whole-rock MgO exceeds 5 wt.%. Plagioclase fractionation is significant in the differentiated rocks with MgO < 5 wt.% (Kawabata et al., 2011).

3. ANALYTICAL METHODS

Rock samples were collected from all the stratigraphic units described above. Petrography, mineral compositions, and whole-rock major and trace element compositions were reported by Kawabata et al. (2011). Isotopic measurements and radiometric dating were conducted for selected samples in this study. The sample locations are shown in Fig. 1.

Sr, Nd, Pb, and Hf isotopic compositions were determined for acid-leached whole-rock powders and clinopyroxene separates, as described in Hanyu et al. (2011a). Sr and Nd isotope ratios were measured with a thermal ionization mass spectrometer (Triton, Thermo–Finnigan) (Hirahara et al., 2009; Takahashi et al., 2009). Sr and Nd isotope ratios were normalized to $^{86}Sr/^{88}Sr = 0.1194$ and $^{146}Nd/^{144}Nd = 0.7219$ to correct for mass fractionation, respectively. Pb isotope ratios were measured with a multiple collector-inductively coupled plasma-mass spectrometer (MC-ICP-MS; Neptune, Thermo–Finnigan) (Kimura and Nakano, 2004; Miyazaki et al., 2009). Mass fractionation factors for Pb were determined using Tl as an external standard. Pb isotope ratios were presented after recalibration using a NIST 981 value of $^{206}Pb/^{204}Pb = 16.9416$, $^{207}Pb/^{204}Pb = 15.5000$ and $^{208}Pb/^{204}Pb = 36.7262$ reported by Baker et al. (2004). Hf isotope ratios were measured on an MC-ICP-MS (IsoProbe; GV Instruments) for 16 whole-rock samples and all clinopyroxene samples, and an MC-ICP-MS (Neptune; Thermo-Finnigan) for 11 whole-rock samples (Hanyu et al., 2011a; Tables 1 and 2). The mass fractionation was determined by $^{179}Hf/^{177}Hf$ and isotope ratios were normalized to a $^{179}Hf/^{177}Hf$ value of 0.7325. The reported $^{176}Hf/^{177}Hf$ ratio is adjusted with reference to a JMC475 value of 0.28216. Duplicate analyses for SH-10 and SH-58 were conducted with both MC-ICP-MS, and the measured Hf isotope ratios show good agreement (Table 2). Sr, Nd, Hf, and Pb isotope ratios measured for international rock standards are presented in Table A1 (Appendix). To determine initial isotope ratios, parent/daughter ratios were measured using single-collector ICP-MS (Agilent 7500ce; Agilent Technologies) for the same leached whole-rock powders and clinopyroxene separates as used for isotope analyses (Chang et al., 2003). The analytical details are shown in Appendix.

He, Ne, and Ar isotope ratios and abundance were determined for coarse-grained olivine and clinopyroxene phenocrysts. Gases were extracted by 150 times pulverization employing the in-vacuum crushing technique. After purification of gases, abundance and isotope ratios of He, Ne and Ar were measured separately on a sector-type noble gas mass spectrometer (GV5400; GV Instruments) (Hanyu et al., 2011b). Abundance of Kr and Xe was determined simultaneously with Ar. All the reported abundance and isotopic data were calibrated by repeated measurements of air and in-house He standards.

The lava eruption ages were determined by applying the K/Ar technique for groundmass handpicked from fine grains and the $^{40}Ar/^{39}Ar$ dating technique for coarsely crushed groundmass. For the K/Ar dating, gases were extracted from the samples by in-vacuum heating and radiogenic ^{40}Ar were measured on a sector-type noble gas mass spectrometer (GV5400; GV Instruments). The $^{40}Ar/^{36}Ar$ ratios and Ar concentrations were normalized through repeated measurements of air standards, and HD-B1 and SORI93B biotite standards (Sato et al., 2005b). Potassium concentrations were determined after acid digestion of the samples on a Zeeman atomic absorption spectrometer (Hitachi Z-5010) (Sato et al., 2005a). For the $^{40}Ar/^{39}Ar$ dating, gases were extracted by stepwise heating from the neutron-irradiated samples with an argon ion continuous laser. Argon isotopes were measured on a custom made mass spectrometer (Research Institute of Natural Sciences, Okayama University of Science; Hyodo, 2008). For details of the method, see Appendix.

4. RESULTS

4.1. $^{40}Ar/^{39}Ar$ and K/Ar ages

K/Ar ages were determined for samples from volcanic units of the NE and SW volcanoes and Late Intrusives. The $^{40}Ar/^{39}Ar$ dating was further conducted in six selected samples to evaluate the results of K/Ar dating. A summary of the $^{40}Ar/^{39}Ar$ ages is presented in Table 3, and the $^{40}Ar/^{39}Ar$ age spectra and K/Ar age data are shown in Fig. A1 and Table A3, respectively, in Appendix. Plateau ages are defined using the following criteria; there are more than two contiguous steps that comprise more than 50% of the total released ^{39}Ar, and the probability of occurrence is higher than 0.05 according to the χ-square test for the ages between the particular steps (Baksi, 2003). In this study, the interpreted ages are also defined when either of the above-mentioned criteria is not achieved. Duplicate analyses showed coherent plateau and interpreted ages within analytical uncertainties (Table 3).

The $^{40}Ar/^{39}Ar$ and K/Ar dating exhibit consistent ages for SH-30, whereas the K/Ar ages for SH-57 and SH-83 are younger than the $^{40}Ar/^{39}Ar$ ages by 0.5–1 Ma (Fig. 2). This is presumably due to Ar loss or K gain caused by low-temperature alteration after emplacement of the lavas because the $^{40}Ar/^{39}Ar$ age spectra contain components with apparently young ages in the low-temperature fractions

Table 1
Measured and age-corrected Sr–Nd–Hf–Pb isotope ratios of whole rock samples.

Sample	SH-10		SH-22	SH-24	SH-25	SH-30	SH-32	SH-35	SH-38	SH-42	SH-43	SH-44B	SH-45	SH-49
Sequence	SW Main	(duplicate)	Late Intru.	SW Lower	SW Lower	Late Intru.	NE Lower	NE Lower	SW Main	Late Intru.	SW Upper	NE Lower	NE Lower	SW Upper
[Measured isotope ratios]														
$^{87}Sr/^{86}Sr$	0.702906		0.712904	0.702940	0.702870	0.703036	0.702829	0.702868	0.702890	0.703573	0.702915	0.703416	0.702861	0.702891
2SE	0.000007		0.000009	0.000007	0.000006	0.000007	0.000006	0.000007	0.000007	0.000007	0.000006	0.000008	0.000007	0.000006
$^{143}Nd/^{144}Nd$	0.512855		0.512853	0.512858	0.512873	0.512862	0.512870	0.512865	0.512858	0.512851	0.512851	0.512884	0.512884	0.512854
2SE	0.000008		0.000012	0.000010	0.000011	0.000012	0.000014	0.000011	0.000009	0.000011	0.000009	0.000009	0.000009	0.000009
$^{176}Hf/^{177}Hf$	0.282880	*0.282889*	*0.282878*	*0.282875*	*0.282913*	*0.282882*	*0.282901*	*0.282886*	*0.282873*	0.282887	0.282880	*0.282893*	*0.282901*	*0.282875*
2SE	0.000009	*0.000010*	0.000010	*0.000011*	*0.000010*	*0.000008*	*0.000009*	*0.000009*	*0.000008*	0.000005	0.000009	*0.000009*	*0.000010*	*0.000009*
$^{206}Pb/^{204}Pb$	20.7744		20.9009	20.6484	20.7113	20.8599	20.7076	20.7762	20.7958	20.8617	20.8180	20.6500	20.7551	20.8472
2SE	0.0008		0.0008	0.0010	0.0008	0.0008	0.0008	0.0009	0.0008	0.0008	0.0007	0.0008	0.0008	0.0007
$^{207}Pb/^{204}Pb$	15.7836		15.7976	15.7723	15.7741	15.7863	15.7734	15.7805	15.7811	15.7892	15.7876	15.7706	15.7770	15.7806
2SE	0.0007		0.0006	0.0008	0.0007	0.0007	0.0007	0.0007	0.0007	0.0007	0.0007	0.0007	0.0007	0.0006
$^{208}Pb/^{204}Pb$	40.0744		40.2643	39.9718	40.0376	40.1341	39.9993	40.0620	40.0503	40.1537	40.0995	40.0593	40.0737	40.0893
2SE	0.0021		0.0019	0.0025	0.0020	0.0019	0.0021	0.0021	0.0020	0.0021	0.0019	0.0020	0.0020	0.0019
[Age corrected isotope ratios]														
Rb (ppm)	14.3		164	11.7	8.6	100	10.2	8.38	11.1	124	44.9	73.3	10.6	22.1
Sr (ppm)	510		5.31	432	339	192	580	256	398	59.9	848	55.8	350	635
$(^{87}Sr/^{86}Sr)_{init}$	0.702896			0.702930	0.702861	0.702866	0.702820	0.702853	0.702879	0.702891	0.702897	0.702795	0.702847	0.702880
Sm (ppm)	3.41		3.91	3.94	3.81	3.66	3.16	3.28	3.09	4.20	1.84	2.92	3.92	3.89
Nd (ppm)	12.7		30.9	14.7	13.9	20.9	11.2	11.7	11.5	26.9	11.0	11.7	14.3	14.5
$(^{143}Nd/^{144}Nd)_{init}$	0.512845		0.512849	0.512848	0.512864	0.512857	0.512857	0.512853	0.512848	0.512846	0.512846	0.512872	0.512872	0.512846
Lu (ppm)	0.210		0.766	0.199	0.210	0.563	0.227	0.187	0.179	0.652	0.143	0.879	0.224	0.239
Hf (ppm)	5.01		29.6	5.79	4.72	20.2	5.42	4.42	4.58	23.1	9.77	18.9	5.76	6.76
$(^{176}Hf/^{177}Hf)_{init}$	0.282879		0.282877	0.282874	0.282912	0.282881	0.282900	0.282885	0.282872	0.282886	0.282880	0.282891	0.282900	0.282874
U (ppm)	0.648		1.81	0.236	0.502	0.773	0.269	0.335	0.500	0.651	1.67	0.358	0.414	0.367
Th (ppm)	0.919		13.2	0.543	1.16	2.43	0.479	0.541	1.29	3.09	4.76	1.91	0.816	0.781
Pb (ppm)	0.763		2.82	0.457	1.20	1.92	0.456	0.535	1.03	2.15	4.01	2.10	0.503	0.943
$(^{206}Pb/^{204}Pb)_{init}$	20.701		20.852	20.604	20.675	20.829	20.643	20.707	20.754	20.839	20.786	20.631	20.665	20.817
$(^{207}Pb/^{204}Pb)_{init}$	15.780		15.795	15.770	15.772	15.785	15.770	15.777	15.779	15.788	15.786	15.770	15.773	15.779
$(^{208}Pb/^{204}Pb)_{init}$	40.040		40.146	39.938	40.010	40.102	39.961	40.025	40.015	40.117	40.070	40.026	40.015	40.068

Sample	SH-58		SH-59	SH-62	SH-70	SH-75	SH-76	SH-77	SH-84	SH-86	SH-90	SH-93	SH-99
Sequence	NE Main	(duplicate)	NE Main	NE Main	Late Intru.	SW Main	SW Main	SW Main	SW Lower	SW Lower	SW Main	Late Intru.	SW Upper
[Measured isotope ratios]													
$^{87}Sr/^{86}Sr$	0.702854		0.702867	0.702865	0.702959	0.702862	0.702904	0.702907	0.702902	0.702870	0.702871	0.702914	0.702907
2SE	0.000006		0.000007	0.000007	0.000006	0.000007	0.000006	0.000007	0.000007	0.000007	0.000007	0.000006	0.000007
$^{143}Nd/^{144}Nd$	0.512864		0.512866	0.512853	0.512862	0.512857	0.512858	0.512857	0.512846	0.512859	0.512853	0.512848	0.512855
2SE	0.000013		0.000015	0.000011	0.000010	0.000008	0.000012	0.000011	0.000007	0.000009	0.000010	0.000009	0.000011
$^{176}Hf/^{177}Hf$	0.282886	*0.282881*	0.282885	0.282885	0.282882	*0.282893*	0.282865	0.282877	*0.282875*	*0.282889*	*0.282874*	*0.282891*	0.282883
2SE	0.000012	*0.000011*	0.000005	0.000006	0.000005	*0.000014*	0.000014	0.000006	*0.000010*	*0.000014*	*0.000011*	*0.000009*	0.000005
$^{206}Pb/^{204}Pb$	20.7063		20.6801	20.6885	20.8444	20.9928	20.8071	20.8082	20.9039	20.8770	20.7439	20.8430	20.8888
2SE	0.0007		0.0009	0.0009	0.0009	0.0009	0.0010	0.0009	0.0009	0.0010	0.0009	0.0009	0.0008
$^{207}Pb/^{204}Pb$	15.7645		15.7644	15.7686	15.7907	15.8083	15.7883	15.7864	15.7988	15.7842	15.7809	15.7913	15.7897
2SE	0.0006		0.0007	0.0007	0.0007	0.0007	0.0007	0.0008	0.0007	0.0009	0.0008	0.0008	0.0007
$^{208}Pb/^{204}Pb$	40.0044		39.9913	40.0176	40.1087	40.2400	40.1112	40.0947	40.1728	40.1239	40.0515	40.1341	40.1218
2SE	0.0020		0.0020	0.0023	0.0021	0.0021	0.0023	0.0022	0.0021	0.0026	0.0022	0.0022	0.0021

Table 1 (*continued*)

Sample	SH-58		SH-59	SH-62	SH-70	SH-75	SH-76	SH-77	SH-84	SH-86	SH-90	SH-93	SH-99
Sequence	NE Main	(duplicate)	NE Main	NE Main	Late Intru.	SW Main	SW Main	SW Main	SW Lower	SW Lower	SW Main	Late Intru.	SW Upper
[Age corrected isotope ratios]													
Rb (ppm)	26.8		50.8	33.5	105	5.01	24.7	64.5	8.48	6.88	10.6	72.0	25.9
Sr (ppm)	877		855	925	557	248	803	586	452	232	352	878	689
$(^{87}Sr/^{86}Sr)_{init}$	0.702842		0.702844	0.702851	0.702897	0.702854	0.702892	0.702866	0.702895	0.702859	0.702860	0.702887	0.702894
Sm (ppm)	4.32		4.08	3.89	2.47	2.79	3.39	4.86	3.20	2.97	3.31	0.735	4.30
Nd (ppm)	17.5		20.1	16.5	14.4	9.8	13.8	26.2	11.8	10.6	11.9	5.07	17.2
$(^{143}Nd/^{144}Nd)_{init}$	0.512855		0.512859	0.512844	0.512857	0.512847	0.512849	0.512850	0.512837	0.512849	0.512843	0.512843	0.512847
Lu (ppm)	0.277		0.324	0.252	0.361	0.152	0.237	0.365	0.190	0.169	0.175	0.050	0.273
Hf (ppm)	7.87		11.5	8.40	17.4	3.89	6.95	15.8	4.84	4.00	4.88	11.4	7.79
$(^{176}Hf/^{177}Hf)_{init}$	0.282885		0.282884	0.282885	0.282882	0.282892	0.282864	0.282877	0.282874	0.282888	0.282873	0.282891	0.282882
U (ppm)	0.998		1.35	0.257	0.284	0.049	0.119	2.26	0.435	0.272	0.150	1.79	1.17
Th (ppm)	2.42		2.45	1.05	1.27	0.242	0.438	5.72	0.951	0.607	0.383	5.64	2.62
Pb (ppm)	2.27		2.73	1.04	9.13	0.142	0.740	4.12	0.978	0.315	0.375	4.09	2.63
$(^{206}Pb/^{204}Pb)_{init}$	20.666		20.635	20.666	20.842	20.963	20.793	20.761	20.865	20.803	20.710	20.809	20.855
$(^{207}Pb/^{204}Pb)_{init}$	15.763		15.762	15.768	15.791	15.807	15.788	15.784	15.797	15.781	15.779	15.790	15.788
$(^{208}Pb/^{204}Pb)_{init}$	39.972		39.964	39.987	40.105	40.192	40.094	40.055	40.145	40.069	40.022	40.099	40.097

Sr and Nd isotope ratios were determined by TIMS. Hf and Pb isotope ratios were determined by MC-ICP-MS.
Hf isotope ratios in italics were determined at ERI, University of Tokyo, and the others were determined at IFREE, JAMSTEC.
Concentrations for parent and daughter elements were determined for leached whole rock powders.
The ages assumed are 11.5 Ma for NE Lower Shield, 9.5 Ma for NE Main Shield, 9 Ma for SW Lower and Main Shields, and 8 Ma for SW Upper Shield and Late Intrusives.

(Fig. A1 in Appendix). Such components were readily eliminated by stepwise heating in the $^{40}Ar/^{39}Ar$ dating but not by single-step fusion in the K/Ar dating. In fact, the samples with low K_2O content (<1.3 wt.%) tend to show erroneously young ages down to 4 Ma presumably due to alteration; therefore, their ages are not reported here. In contrast, SH-44B shows the K/Ar age (12.13 ± 0.49 Ma) older than the $^{40}Ar/^{39}Ar$ age (10.68 ± 0.15 Ma). This sample is a trachyte fragment in a submarine breccia from the NE Lower Shield. We attribute the apparent age discrepancy to the heterogeneous distribution of excess ^{40}Ar in the rocks that erupted in the submarine environment.

The problem of excess ^{40}Ar seems to exist in the previous K/Ar dating efforts as well. The oldest rock dated at 14.6 and 14.0 Ma (Sample No. 679) by Baker et al. (1967) was collected from the NE Lower Shield, the lowest stratigraphic level among the accessible parts of the island. However, the $^{40}Ar/^{39}Ar$ ages of samples collected from the same unit are much younger (10.7–11.8 Ma; SH-32 and SH-44B; Fig. 2). Since Sample No. 679 was a basalt with pyroxene, feldspar, and olivine (Baker et al., 1967), the apparent K/Ar ages in the bulk sample might have been modified to older values due to the presence of excess ^{40}Ar in the phenocrysts. Previously reported K/Ar ages of samples from the NE Main, SW Lower, and SW Main Shields are also systematically older by 1–2 Ma than the $^{40}Ar/^{39}Ar$ ages in this study. This is also ascribed to excess ^{40}Ar from the olivine and clinopyroxene phenocrysts in the highly phyric rocks. In fact, our data are in agreement with the K/Ar ages of Baker et al. (1967) for samples from the Late Intrusives presumably because they are typically aphyric. The problem of excess ^{40}Ar had not been recognized in the 1960s.

The age for each stratigraphic unit must be revised by the $^{40}Ar/^{39}Ar$ ages. However, several implications stated by Baker et al. (1967) regarding the volcanic growth history remain valid. The submarine NE Lower Shield must be older than 10.7 Ma (SH-44B), which predates the subaerial NE Main Shield. This fact precludes the claim by Chaffey et al. (1989) for a much more restricted age variation (7–9 Ma), based on their preliminary age data. The $^{40}Ar/^{39}Ar$ ages of the Lower and Main Shields of the SW volcano (SH-38, SH-83) overlap with the ages of the Main Shield of the NE volcano. This suggests that the early volcanic activity occurred in the northeast corner of the island in the submarine environment, and then the eruption center migrated southwestward within a million years, resulting in forming coalesced volcanic edifices. Finally, the activity associated with the Late Intrusives occurred from 9 to 7 Ma after the shield volcanism (Fig. 2).

4.2. Radiogenic isotopes and noble gases

Sr, Nd, Pb, and Hf isotopic compositions of whole-rock powders and clinopyroxene separates determined in this study overlap with those previously reported from St. Helena (Tables 1 and 2; Fig. 3). The measured $^{87}Sr/^{86}Sr$ values range from 0.70282 to 0.70357, except for SH-22 whole-rock. After the age correction, the initial $^{87}Sr/^{86}Sr$ for all the samples but SH-22 fall within a narrow range between 0.70280 and 0.70293 (Table 1). SH-22, a trachyte

Table 2
Measured and age-corrected Sr–Nd–Hf–Pb isotope ratios of clinopyroxene samples.

Sample	SH-10	SH-24	SH-25	SH-32	SH-35	SH-38	SH-45	SH-75	SH-84	SH-86	SH-90
Sequence	SW Main	SW Lower	SW Lower	NE Lower	NE Lower	SW Main	NE Lower	SW Main	SW Lower	SW Lower	SW Main
[Measured isotope ratios]											
$^{87}Sr/^{86}Sr$	0.702860	0.702913	0.702890	0.702818	0.702832	0.702865	0.702846	0.702847	0.702879	0.702844	0.702863
2SE	0.000006	0.000006	0.000007	0.000007	0.000007	0.000007	0.000007	0.000007	0.000007	0.000007	0.000007
$^{143}Nd/^{144}Nd$	0.512865	0.512859	0.512861	0.512884	0.512872	0.512872	0.512877	0.512862	0.512856	0.512862	0.512866
2SE	0.000006	0.000004	0.000004	0.000003	0.000006	0.000005	0.000005	0.000004	0.000004	0.000005	0.000004
$^{176}Hf/^{177}Hf$	*0.282893*	*0.282876*	*0.282886*	*0.282908*	*0.282888*	*0.282877*	*0.282889*	*0.282882*	*0.282871*	*0.282879*	*0.282877*
2SE	*0.000008*	*0.000009*	*0.000009*	*0.000008*	*0.000008*	*0.000008*	*0.000008*	*0.000009*	*0.000008*	*0.000010*	*0.000009*
$^{206}Pb/^{204}Pb$		20.6484	20.6767	20.7292	20.7256	20.7688	20.7176	20.9295	20.9062	20.8051	20.7152
2SE		0.0011	0.0013	0.0011	0.0011	0.0011	0.0010	0.0011	0.0010	0.0013	0.0011
$^{207}Pb/^{204}Pb$		15.7760	15.7737	15.7744	15.7791	15.7883	15.7780	15.8048	15.7999	15.7905	15.7802
2SE		0.0009	0.0011	0.0010	0.0009	0.0009	0.0009	0.0009	0.0008	0.0011	0.0010
$^{208}Pb/^{204}Pb$		39.9819	40.0154	40.0100	40.0511	40.0625	40.0619	40.1745	40.1920	40.1109	40.0346
2SE		0.0028	0.0033	0.0028	0.0027	0.0027	0.0028	0.0025	0.0024	0.0031	0.0028
[Age corrected isotope ratios]											
Rb (ppm)	0.181	1.07	0.588	0.534	0.727	0.331	0.417	0.248	0.942	0.157	0.530
Sr (ppm)	62.6	80.0	59.8	64.3	66.3	69.1	70.0	63.0	73.3	48.7	73.5
$(^{87}Sr/^{86}Sr)_{init}$	0.702859	0.702908	0.702886	0.702814	0.702827	0.702863	0.702843	0.702845	0.702875	0.702843	0.702860
Sm (ppm)	3.42	3.05	3.09	4.28	3.37	4.17	4.01	3.68	4.01	2.23	4.41
Nd (ppm)	10.6	10.2	9.69	13.1	10.9	13.9	13.0	13.3	13.2	7.11	14.1
$(^{143}Nd/^{144}Nd)_{init}$	0.512853	0.512849	0.512849	0.512869	0.512858	0.512861	0.512863	0.512852	0.512846	0.512851	0.512855
Lu (ppm)	0.143	0.123	0.132	0.188	0.143	0.184	0.166	0.168	0.171	0.095	0.185
Hf (ppm)	2.44	2.26	2.08	2.87	2.59	3.04	3.27	2.03	2.86	1.37	3.43
$(^{176}Hf/^{177}Hf)_{init}$	0.282891	0.282874	0.282884	0.282906	0.282886	0.282875	0.282887	0.282880	0.282870	0.282877	0.282875
U (ppm)		0.067	0.068	0.040	0.037	0.037	0.034	0.020	0.053	0.013	0.046
Th (ppm)		0.227	0.144	0.144	0.147	0.142	0.140	0.123	0.193	0.059	0.187
Pb (ppm)		0.138	0.088	0.089	0.105	0.112	0.073	0.090	0.102	0.033	0.144
$(^{206}Pb/^{204}Pb)_{init}$		20.606	20.609	20.680	20.687	20.740	20.667	20.910	20.862	20.771	20.688
$(^{207}Pb/^{204}Pb)_{init}$		15.774	15.771	15.772	15.777	15.787	15.776	15.804	15.798	15.789	15.779
$(^{208}Pb/^{204}Pb)_{init}$		39.935	39.969	39.951	40.000	40.026	39.993	40.136	40.138	40.060	39.998

Sr and Nd isotope ratios were determined by TIMS. Hf and Pb isotope ratios were determined by MC-ICP-MS.
Hf isotope ratios in italics were determined at ERI, University of Tokyo.
Concentrations for parent and daughter elements were determined for leached clinopyroxene samples.
The ages assumed are 11.5 Ma for NE Lower Shield, and 9 Ma for SW Lower and Main Shields.

Table 3
$^{40}Ar/^{39}Ar$ ages of St. Helena samples.

Sample	Sequence	Total age			Plateau	Interpreted age			
		N[a]	Age (Ma)	Error (2s)		N[a]	%^{39}Ar	Age (Ma)	Error (2s)
SH-30-1	Late Intrusives	7	8.24	0.29		3	39.9	8.79	0.34
SH-30-2*		6	8.28	0.36	P	5	92.8	8.73	0.28
SH-32-1	NE Lower Shield	6	10.50	0.88	P	4	91.5	11.49	0.75
SH-32-2*		6	7.22	1.02	P	3	68.7	11.76	0.94
SH-38-1	SW Main Shield	8	7.49	1.04		4	67.0	10.55	0.40
SH-38-2*		6	9.62	0.83		-			
SH-44B-2	NE Lower Shield	7	10.23	0.21		5	84.6	10.68	0.15
SH-57-1	NE Main Shield	6	6.82	0.30		3	52.5	9.75	0.35
SH-57-2*		6	8.27	0.99	P	3	96.8	9.50	0.56
SH-83-1	SW Lower Shield	6	7.18	0.33	P	3	82.3	9.08	0.32
SH-83-2*		11	4.55	0.43		5	53.4	9.46	0.32

Plateau ages are defined by the following criteria; there are more than two contiguous steps that comprise >50% of the total ^{39}Ar released, and probability of occurrence is more than 0.95 by Chi square test.
* Duplicate analyses.
[a] Number of stepwise fractions used for age calculation.

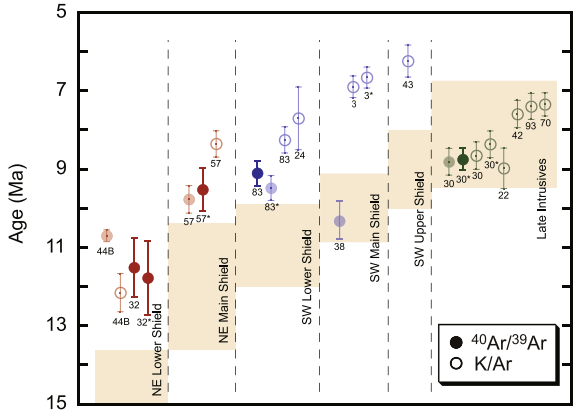

Fig. 2. $^{40}Ar/^{39}Ar$ and K/Ar ages of lava flows and dykes. Solid and open symbols with sample numbers represent ages determined by $^{40}Ar/^{39}Ar$ and K/Ar dating, respectively. The asterisk next to the sample numbers indicates duplicate data. Color codes are red for shield lavas from the NE volcano, blue for shield lavas from the SW volcano, and green for the Late Intrusives. The dark and light colored symbols for $^{40}Ar/^{39}Ar$ data denote plateau and interpreted ages, respectively. Error bars correspond to 2σ. Orange fields indicate the range of previous K/Ar age data from Abdel-Monem and Gast (1967) and Baker et al. (1967), recalculated with the decay constants for ^{40}K to ^{40}Ar (0.581×10^{-10}/year) and ^{40}Ca (4.962×10^{-10}/year), and ^{40}K content of potassium (1.167×10^{-4}) of Steiger and Jäger (1977). (For interpretation of the references to color in this figure legend, the reader is referred to the web version of this article.)

from the Late Intrusives, has extremely high $^{87}Sr/^{86}Sr$ (0.71290) and Rb/Sr (31). It was difficult to determine the initial $^{87}Sr/^{86}Sr$ for this sample because it is highly dependent on the assumed age. Conversely, this sample may provide an age constraint. Assuming an initial $^{87}Sr/^{86}Sr$ of 0.70287–0.70290 determined by the other samples from the Late Intrusives, the calculated age is about 7.9 Ma, which is consistent with the $^{40}Ar/^{39}Ar$ and K/Ar ages of the Late Intrusives. Note that the age correction for $^{87}Sr/^{86}Sr$ was conducted with Rb/Sr in the leached whole-rocks, the same powders used for isotope measurements. If we use Rb/Sr in the unleached whole-rocks, $^{87}Sr/^{86}Sr$ of the differentiated samples, SH-22 and SH-42, are changed from the measured values of 0.71290 and 0.70357 to the corrected values of 0.70961 and 0.70312, respectively, which seems to lead to insufficient correction. For the other samples, age correction using Rb/Sr in the leached and unleached whole-rocks do not yield significant difference in the age-corrected $^{87}Sr/^{86}Sr$, which is up to 0.000008.

The maximum radiogenic ingrowth for $^{143}Nd/^{144}Nd$ and $^{176}Hf/^{177}Hf$ since crystallization of the magmas is 0.000015 and 0.000002, respectively. Therefore, its effect is negligibly small relative to the overall variations in the Nd and Hf isotope ratios observed in the St. Helena lavas (Fig. 3a,b). In contrast, the radiogenic ingrowth for Pb isotopes cannot be disregarded; for example, the maximum $^{206}Pb/^{204}Pb$ ingrowth was 0.091 (SH-45 whole-rock), which corresponds to nearly one fourth of the $^{206}Pb/^{204}Pb$ variation observed in the St. Helena lavas. Consequently, age-correction is necessary to precisely determine the Pb isotopic trends (Hanyu et al., 2011a).

The samples do not show any systematic difference in age-corrected isotope ratios between whole-rocks and clinopyroxene separates from the same rocks. Moreover, clinopyroxene/whole-rock concentration ratios for rare earth elements and incompatible elements overlap with the partition coefficients between clinopyroxenes and basaltic melts (Fig. A2 in Appendix). This fact indicates that the clinopyroxenes are not xenocrysts and that isotopic compositions were not modified by posteruption weathering or crustal assimilation after clinopyroxene crystallization (Hanyu and Nakamura, 2000; Jackson et al., 2009; Hanyu et al., 2011a). Crustal assimilation before clinopyroxene crystallization is also unlikely because the initial $^{87}Sr/^{86}Sr$ are remarkably uniform among the samples, the rock types of which range from alkali basalts to differentiated trachytes. Since Sr isotope ratios are more susceptible to assimilation of hydrothermally altered crustal material than Nd, Hf, and Pb isotopes (Dupré et al., 1982; Millet et al., 2008; Hanyu

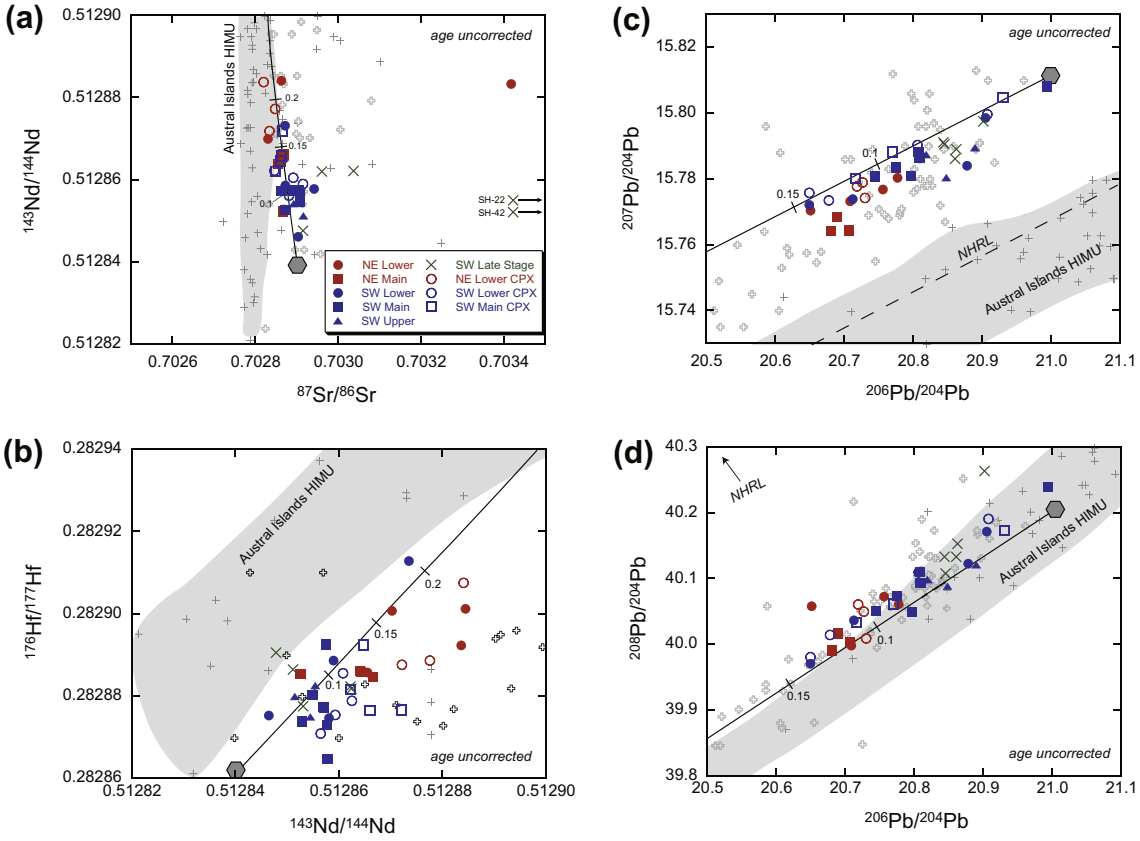

Fig. 3. Age-uncorrected Pb, Sr, Nd, and Hf isotope ratios. Color codes for the plots are the same as in Fig. 2. Solid symbols and crosses denote whole-rock data. Open symbols denote data from clinopyroxene separates. Previous isotopic data for St. Helena are shown by gray bold crosses (Sun, 1980; White and Hofmann, 1982; Newsom et al., 1986; Chaffey et al., 1989; Graham et al., 1992; Salters and White, 1998; Salters et al., 2011; Thirlwall, 2000). The isotopic data and their range for the Austral Islands HIMU lavas are shown by gray thin crosses and the gray field for comparison (Hanyu et al., 2011a and references therein). The northern hemisphere reference line (NHRL) in (c) is from Hart (1984). NHRL in (d) is outside the range of the figure. The black solid lines indicate mixing lines between melt with the most HIMU-like enriched isotopic compositions among the St. Helena lavas and melt derived from the depleted component. The mixing fractions of the depleted melt are annotated on the lines. The isotopic compositions of the HIMU-like melt are assumed to be; $^{87}Sr/^{86}Sr = 0.70290$, $^{143}Nd/^{144}Nd = 0.51284$, $^{176}Hf/^{177}Hf = 0.28286$, $^{206}Pb/^{204}Pb = 21.00$, $^{207}Pb/^{204}Pb = 15.81$, $^{208}Pb/^{204}Pb = 40.20$ (gray hexagon). Sr, Nd, Hf, and Pb concentrations in the HIMU-like melt are taken from average compositions of primary melts in St. Helena (Kawabata et al., 2011). The isotopic compositions of the depleted component are assumed to be; $^{87}Sr/^{86}Sr = 0.70270$, $^{143}Nd/^{144}Nd = 0.51305$, $^{176}Hf/^{177}Hf = 0.28312$, $^{206}Pb/^{204}Pb = 18.50$, $^{207}Pb/^{204}Pb = 15.58$, $^{208}Pb/^{204}Pb = 38.50$. Sr, Nd, Hf, and Pb concentrations in the depleted component are taken from the values of the MORB source mantle (Salters and Stracke, 2004), and those in the melt are calculated by assuming 1% partial melting in the garnet stability field after Hanyu et al. (2011a). (For interpretation of the references to color in this figure legend, the reader is referred to the web version of this article.)

et al., 2011a), crustal assimilation cannot be responsible for the Nd, Hf, and Pb isotopic variations observed in the studied samples.

No notable correlations between isotope ratios and trace element compositions were found in the samples. Although trace element abundance are different between basalts, trachybasalts, and trachytes, several key trace element ratios, such as Ba/Nb, Zr/Sm, and Tb/Yb, are uniform irrespective of isotope ratios and major element compositions (Fig. 4; Kawabata et al., 2011). Chaffey et al. (1989) pointed out possible covariations for $^{206}Pb/^{204}Pb$ and $^{143}Nd/^{144}Nd$ with La/Yb and Sm/Nd, respectively. However, we do not recognize such correlations in the present dataset. Instead, La/Yb and Sm/Nd are likely controlled by partial melting, crystal fractionation, and accumulation because they correlate with MgO, SiO_2, and K_2O rather than with isotope ratios.

Although the isotopic variations observed in the St. Helena lavas are best explained by two-component mixing as discussed below, small variation in isotope ratios (e.g., $^{206}Pb/^{204}Pb$ ranging from 20.6 to 21.0) suggest that mixing proportions are rather constant.

Noble gas isotope ratios and abundance in olivine and clinopyroxene separates are shown in Table 4. The samples from the NE and SW volcanoes exhibit limited variation in $^{3}He/^{4}He$ between 5.24 and 5.97 Ra (Ra; $^{3}He/^{4}He$ normalized to the atmospheric ratio). Olivine and clinopyroxene separates from SH-24 show good agreement in $^{3}He/^{4}He$. $^{3}He/^{4}He$ measured in this study overlap with previously reported $^{3}He/^{4}He$ values for St. Helena (4.25–5.87; Graham

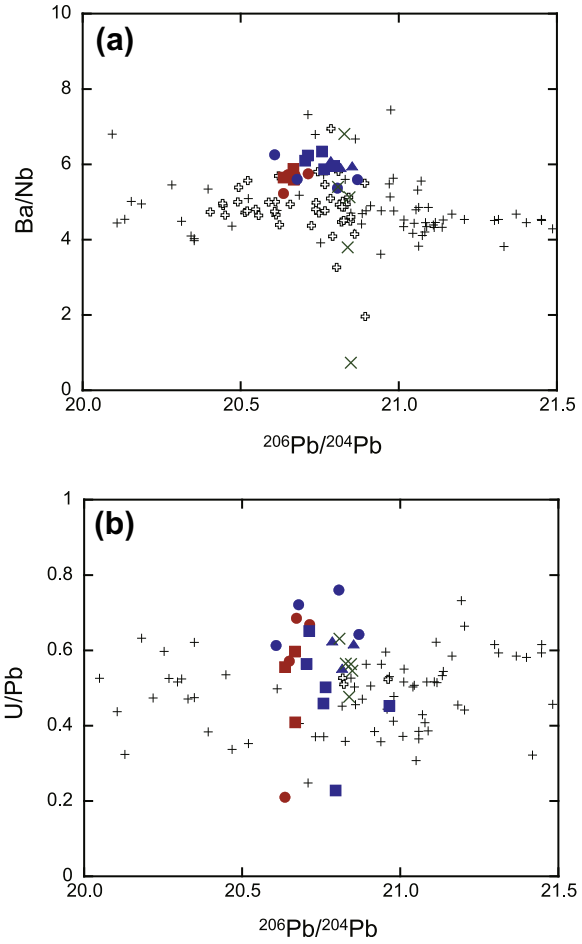

Fig. 4. Plots of $^{206}Pb/^{204}Pb$ versus (a) Ba/Nb and (b) U/Pb. Symbols are the same as in Fig. 3. Data for St. Helena lavas are from Newsom et al. (1986) and Chaffey et al. (1989). Data for Austral Islands lavas are from Dupuy et al. (1988), Hauri and Hart (1993), Woodhead (1996), Chauvel et al. (1992, 1997), Kogiso et al. (1997b), and Hanyu et al. (2011a, 2013).

et al., 1992), confirming that the St. Helena lavas have lower $^{3}He/^{4}He$ than typical MORB. Ne isotope ratios were indistinguishable from atmospheric values within 1σ analytical uncertainties. The $^{40}Ar/^{36}Ar$ values were less than 600 for all the samples but SH-45 from the NE Lower Shield. The relatively low $^{40}Ar/^{36}Ar$ might be due to atmospheric or crustal contamination, although no clear variation between $^{40}Ar/^{36}Ar$ and ^{36}Ar abundance is observed. Clinopyroxene separates from SH-24 exhibit lower $^{40}Ar/^{36}Ar$ than olivine separates from the same rock.

5. DISCUSSION

5.1. Geochemical variations of the St. Helena lavas

The St. Helena lavas exhibit isotopic compositions that are unique to HIMU with radiogenic Pb and unradiogenic Sr isotopes (Sun, 1980; Chaffey et al., 1989; Reisberg et al., 1993) (Fig. 3a,c,d). The St. Helena lavas have relatively low $^{176}Hf/^{177}Hf$ for a given $^{143}Nd/^{144}Nd$, and plot below the Nd–Hf isotope array defined by the majority of OIB and MORB (Fig. 3b; Salters et al., 2011). The isotopic variations in the St. Helena lavas are small, but the isotopic compositions systematically change between volcanic units from the NE and the SW volcanoes (Chaffey et al., 1989). The lavas from the NE volcano tend to show less radiogenic Pb isotopes associated with more radiogenic Nd and Hf isotopes as a group compared to those from the SW volcano. The isotopic variations become larger during the formation of the Lower and Main Shields of the SW volcano. Towards the last volcanic stages recorded in the SW Upper Shield and Late Intrusives, the isotopic compositions are confined within narrow fields with more radiogenic Pb, and less radiogenic Nd and Hf isotopes.

According to Chaffey et al. (1989), the isotopic variations reflect two-component mixing between materials from the HIMU component and the depleted mantle component, which is confirmed by the present data. The mixing relation is likely influenced by the melting characteristics of the source components (Ito and Mahoney, 2005; Stracke and Bourdon, 2009). If the material from the HIMU component had lower solidus than the depleted mantle source, the HIMU melt would be diluted by the melt from the depleted mantle during the shield-building stage when the plume heat flux was robust. Given the apparently constant fractions of the HIMU component and the depleted component supplied to the melting region from a mantle plume, the decline of the heat flux would suppress the production of depleted melt, and consequently, the lavas would show strong HIMU geochemical signatures in the late stage of the volcanic activity (Chaffey et al., 1989).

The isotopic variations can be reproduced by a simple mixing model. Fig. 3 shows mixing lines between melt with the most HIMU-like enriched isotopic compositions and melt derived from the depleted component (see the caption of Fig. 3 for the compositions of the mixing components). Assuming 1% partial melting of the depleted component in the garnet stability field, the isotopic variations observed in the St. Helena lavas are accounted for by the addition of such depleted melt by approximately 20% to the HIMU-like melt. In reality, the melting relationships in the multi-component system should be more complex (Ito and Mahoney, 2005; Stracke and Bourdon, 2009), but small change in mixing fractions could yield the observed isotopic variations.

Trace element ratios do not show clear temporal or geographical variation in the St. Helena lavas. Low Ba/Nb and high U/Pb are the features unique to the HIMU lavas among OIB (Willbold and Stracke, 2006), but no correlation between isotope ratios and these trace element ratios is observed (Fig. 4). At Tubuai in Austral Islands, some submarine lavas with less radiogenic Pb isotopes ($^{206}Pb/^{204}Pb \sim 19.6$) exhibit different trace element compositions from subaerial lavas with radiogenic Pb isotopes ($^{206}Pb/^{204}Pb \sim 21.0$) because mixing fractions of the HIMU component against the depleted component were different between these lavas (Hanyu et al., 2013). Considering the limited range of mixing ratios suggested by the small $^{206}Pb/^{204}Pb$ variation (20.6–21.0) in the St. Helena lavas, the variations in incompatible element ratios would be also

Table 4
Noble gas isotopic compositions of olivine and clinopyroxene samples.

Sample	Unit	Weight (g)	Abundance (cm^3STP/g)	^{4}He ($\times10^9$)	^{20}Ne ($\times10^{12}$)	^{36}Ar ($\times10^{12}$)	^{84}Kr ($\times10^{12}$)	^{132}Xe ($\times10^{12}$)	^{3}He/^{4}He (Ra)	Error (1σ)	^{20}Ne/^{22}Ne	Error (1σ)	^{21}Ne/^{22}Ne	Error (1σ)	^{38}Ar/^{36}Ar	Error (1σ)	^{40}Ar/^{36}Ar	Error (1σ)
SH-10 cpx	SW Main	1.016		28.7	1177	2772	84.7	1.07	5.97	0.15	9.86	0.02	0.0290	0.0002	0.189	0.001	306.2	0.5
SH-24 olivine	SW Lower	0.470		58.0		68.2	2.48	0.055	5.55	0.18					0.189	0.002	445.4	1.5
SH-24 cpx	SW Lower	1.073		15.7	215	196	13.6	0.321	5.32	0.25	9.92	0.03	0.0293	0.0005	0.190	0.001	315.5	0.5
SH-25 olivine	SW Lower	1.032		27.4	42.8	64.8	2.33	0.046	5.63	0.23	9.73	0.07	0.0287	0.0009	0.189	0.001	552.7	1.0
SH-32 cpx	NE Lower	1.018		16.0	50.8	113	4.34	0.070	5.67	0.20					0.189	0.001	353.3	0.5
SH-35 olivine	NE Lower	0.720		36.3	31.8	121	6.37	0.151	5.77	0.23					0.189	0.001	575.5	0.8
SH-38 olivine	SW Main	0.810		11.6	46.9	49.6	1.43	0.028	5.91	0.28					0.188	0.002	371.8	0.8
SH-45 olivine	NE Lower	0.852		22.5	67.6	52.3	1.40	0.029	5.24	0.30	9.74	0.06	0.0302	0.0009	0.188	0.002	1677	4
SH-75 cpx	SW Main	1.304		26.6	676	829	16.6	0.120	5.66	0.22	9.81	0.02	0.0288	0.0002	0.189	0.001	316.9	0.4
SH-84 olivine	SW Lower	1.304		19.1	12.2	15.4	1.05	0.021	5.74	0.25					0.203	0.002	598.5	1.6
SH-86 olivine	SW Lower	1.051		6.32	13.5	94.5	4.71	0.157	5.59	0.35					0.189	0.001	339.2	0.7
SH-90 olivine	SW Main	1.036		11.4	50.1	130	4.70	0.088	5.89	0.27					0.189	0.001	316.9	0.8

All samples were pulverized over 150 crushing strokes for gas extraction.

small. Moreover, at ocean island settings, the degree of partial melting is expected to be low because the melting region is confined deep beneath the lithospheric lid. In this case, small variation in the melting degree would give rise to significant change in trace element compositions and melt production rates of the mixing components, which would obscure simple mixing relationships in terms of trace elements (Ito and Mahoney, 2005; Stracke and Bourdon, 2009).

5.2. Similarity between the HIMU lavas from St. Helena and Austral Islands

The HIMU lavas from Austral Islands exhibit nearly vertical arrays in $^{87}Sr/^{86}Sr$–$^{143}Nd/^{144}Nd$ space, and positively correlated but oblique arrays to the MORB–OIB array in $^{143}Nd/^{144}Nd$–$^{176}Hf/^{177}Hf$ space, like the St. Helena lavas (Chauvel et al., 1992; Hémond et al., 1994; Woodhead, 1996; Kogiso et al., 1997b; Schiano et al., 2001; Lassiter et al., 2003; Hanyu et al. 2011a, 2013; Salters et al., 2011) (Fig. 3a and b). Moreover, both HIMU lavas show overlapping trends in $^{206}Pb/^{204}Pb$–$^{208}Pb/^{204}Pb$ space (Fig. 3d).

Hanyu et al. (2011a) attributed the Austral Islands arrays to mixing between the two materials; one from an upwelling plume material from the HIMU component and the other from the ambient depleted mantle entrained by or interacting with the plume. The involvement of depleted mantle in the Austral Islands HIMU lavas was further confirmed by the submarine basalts from Rurutu, Tubuai, and Raivavae, in which the isotopic arrays extend close to the Pacific MORB field (Hanyu et al., 2013).

The isotopic arrays defined by the St. Helena and Austral Islands HIMU lavas partly overlap with each other in $^{87}Sr/^{86}Sr$–$^{143}Nd/^{144}Nd$ and $^{143}Nd/^{144}Nd$–$^{176}Hf/^{177}Hf$ spaces. Indeed, the fact that the St. Helena lavas have slightly higher $^{87}Sr/^{86}Sr$ (~0.0001) and lower $^{176}Hf/^{177}Hf$ (~0.00003) for a given $^{143}Nd/^{144}Nd$ than the Austral Islands lavas probably reflects the different evolution of the two HIMU reservoirs beneath St. Helena in the Atlantic and Austral Islands in the Pacific (Fig. 3a and b). However, assuming a reservoir formation age of 2 Ga, the difference in Rb/Sr of 0.001 and Lu/Hf of 0.006 would be sufficient to account for the Sr and Hf isotopic difference between the two reservoirs, while typical oceanic crust including fresh and altered MORB and gabbro show much larger ranges in Rb/Sr and Lu/Hf of 0.004–0.08 and 0.17–0.22, respectively (Stracke et al., 2003). We prefer to emphasize how small such differences are, considering the existing models that the HIMU reservoir(s) may have formed by subduction of either altered oceanic crust or metasomatized lithosphere, both of which should be geochemically heterogeneous (Stracke et al., 2005; Stracke, 2012).

Also, the HIMU lavas from St. Helena and Austral Islands show similar and unique trace element abundance patterns when normalized to primitive mantle values: (1) negative slope between La and Lu; (2) positive slope between Rb and Nb; and (3) depletion in fluid-mobile elements, such as K, Pb, and Sr (Willbold and Stracke, 2006; Kawabata et al., 2011). The first characteristic is common to many OIB, and is ascribed to low-degree partial melting with residual garnet in the source. The second and third characteristics are indigenous to the HIMU lavas. Because depletion in highly incompatible elements (Rb to Nb) is a feature of MORB, the second characteristics are best explained by the involvement of subducted oceanic crust in the HIMU component. However, the third characteristics are not typical for MORB. The depletion of fluid-mobile elements in the HIMU lavas is mirrored by the enrichment of these elements in subduction-zone magmas. Consequently, the third characteristics are ascribed to selective extraction of fluid-mobile elements from hydrated altered oceanic crust via subduction dehydration (Dupuy et al., 1988; Weaver, 1991; Chauvel et al., 1992, 1995; Woodhead, 1996; Kogiso et al., 1997a; Stracke et al., 2003, 2005; Willbold and Stracke, 2006; Hanyu et al., 2011a; Kawabata et al., 2011). This model is consistent with the He–Ne–Ar systematics that document enrichment in U relative to fluid-mobile K in the HIMU component (Hanyu et al., 2011b).

During subduction, Pb is more mobile than U and Th in the presence of fluids (Keppler, 1996; Kogiso et al., 1997a). Accordingly, the dehydrated residue would possess elevated U/Pb and Th/Pb that would give rise to radiogenic Pb isotopic compositions after billions of years, as required for the HIMU component (Chauvel et al., 1992; Kogiso et al., 1997b; Becker et al., 2000; Stracke et al., 2003). In contrast, rare earth elements and high-field strength elements are less mobile during hydrothermal alteration and subduction dehydration (Staudigel et al., 1996; Kogiso et al., 1997a; Becker et al., 2000; Bach et al., 2003), and therefore Nd and Hf isotopes are less susceptible to these processes. The HIMU lavas from St. Helena and Austral Islands show uniquely low $^{143}Nd/^{144}Nd$ for a given $^{176}Hf/^{177}Hf$ compared to the correlation line defined by other OIB and MORB in Nd–Hf isotope space (Chauvel et al., 1992; Salters and White, 1998; Lassiter et al., 2003; Salters et al., 2011; Hanyu et al., 2011a). This feature is consistent with the subducted oceanic crust and lithosphere being the precursor of the HIMU component, because MORB and gabbro in the oceanic crust show lower Lu/Hf and Sm/Nd that those in the MORB source (Salters and White, 1998; Chauvel et al., 2008).

The HIMU lavas show $^{87}Sr/^{86}Sr$ similarly unradiogenic to MORB. The vertical mixing array in $^{87}Sr/^{86}Sr$–$^{143}Nd/^{144}Nd$ space is interpreted as that the HIMU component has either unradiogenic $^{87}Sr/^{86}Sr$ or much lower Sr/Nd than the depleted component. However, the latter possibility seems unlikely because Sr/Nd in the HIMU lavas fall within the range defined by other OIB, indicating no selective depletion in Sr relative to Nd in the HIMU component (Willbold and Stracke, 2006). In addition, Sr and Nd are not expected to be significantly fractionated from each other by partial melting because of their similar incompatibility. Therefore, unradiogenic $^{87}Sr/^{86}Sr$ is a characteristic feature of the HIMU component.

If the HIMU precursor was ancient hydrothermally altered oceanic crust, it may have variable and more radiogenic $^{87}Sr/^{86}Sr$ than those expected in the HIMU lavas, because hydrothermal fluids imprint high Rb/Sr on the

altered oceanic crust (Staudigel et al., 1996; Bach et al., 2001, 2003; Kelley et al., 2003). Consequently, unradiogenic $^{87}Sr/^{86}Sr$ requires an additional process for reducing Rb/Sr in the recycled altered oceanic crust, that is, fluid dehydration through subduction. High-pressure experiments and studies of natural eclogites demonstrate significant loss of Rb relative to Sr (Keppler, 1996; Kogiso et al., 1997a; Becker et al., 2000). Bach et al. (2003) suggested that removal of 40–55% Rb and 40% Sr from the model altered MORB, deduced from the drill cores at Sites 504B and 417/418, can maintain unradiogenic $^{87}Sr/^{86}Sr$ in the oceanic crust subducted 1–2 billion years ago. Another notable point is the initial $^{87}Sr/^{86}Sr$ of the recycled oceanic crust, which may uptake radiogenic $^{87}Sr/^{86}Sr$ from seawater (~0.709 at present) during hydrothermal alteration. The major host of seawater-derived Sr is carbonate that is concentrated in the upper layer in the oceanic crust (Bach et al., 2001). Considering bulk oceanic crust including highly altered upper layer and less altered lower layer, it may have nominal excess of $^{87}Sr/^{86}Sr$ from the depleted mantle value as a whole. Moreover, it is worth mentioning that $^{87}Sr/^{86}Sr$ in the ancient seawater was not as radiogenic as that in the modern seawater (Shields and Veizer, 2002). The seawater Sr isotope secular variation indicates that a monotonous increase of $^{87}Sr/^{86}Sr$ away from mantle-like value (~0.701) started at ~2.5 Ga and continued until ~1.8 Ga when $^{87}Sr/^{86}Sr$ reached ~0.7045. Consequently, the initial $^{87}Sr/^{86}Sr$ of the altered oceanic crust in the Archean and early Proterozoic, even if its Sr were completely replaced by seawater-derived Sr, would be lower than $^{87}Sr/^{86}Sr$ observed in the present-day HIMU lavas and MORB (Woodhead, 1996).

5.3. Difference between the HIMU lavas from St. Helena and Austral Islands

The HIMU lavas from St. Helena and Austral Islands exhibit systematic differences in Pb and He isotopes. The St. Helena lavas plot away from the trend defined by the Austral Islands HIMU lavas in $^{206}Pb/^{204}Pb$–$^{3}He/^{4}He$ space (Fig. 5). The negative correlation between $^{206}Pb/^{204}Pb$ and $^{3}He/^{4}He$ observed in the Austral Islands HIMU lavas is best explained by the mixing the HIMU component with radiogenic He isotopes and the depleted component with MORB-like $^{3}He/^{4}He$ (Parai et al., 2009; Hanyu et al., 2011b). Although the St. Helena lavas do not show a linear trend due to small isotopic variations, the low-$^{3}He/^{4}He$ signature shared by the St. Helena and Austral Islands HIMU lavas is ascribed to the radiogenic He expected in the recycled materials (Graham et al., 1992; Hanyu and Kaneoka, 1997; Parai et al., 2009). Note that "young-HIMU" lavas from Canary Islands show $^{3}He/^{4}He$ close to the MORB values (Fig. 5). The Pb and He isotopes of the Canary Islands lavas cannot be explained by mixing the "old-HIMU" component and the depleted component because they tend to show uniquely low $^{207}Pb/^{204}Pb$ for a given $^{206}Pb/^{204}Pb$ relative to the HIMU lavas from St. Helena and Austral Islands (see Section 5.4). Day and Hilton (2011) suggested that the $^{3}He/^{4}He$ signature in OIB is controlled by the He content in the mixing components, which may give rise to decoupling between noble gases and radiogenic isotopes.

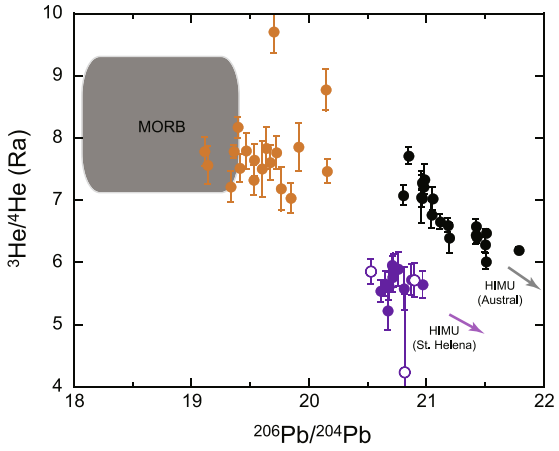

Fig. 5. Plots of $^{206}Pb/^{204}Pb$ versus $^{3}He/^{4}He$. Purple symbols with open and closed circles demote data for St. Helena lavas from Graham et al. (1992) and this study, respectively. Black and orange circles denote data for HIMU lavas from Austral Islands (Parai et al., 2009; Hanyu et al., 2011b) and Canary Islands (Day and Hilton, 2011), respectively. Error bars correspond to 1σ. (For interpretation of the references to color in this figure legend, the reader is referred to the web version of this article.)

Similarly, the St. Helena lavas have distinctly higher $^{207}Pb/^{204}Pb$ for a given $^{206}Pb/^{204}Pb$ than the Austral Islands lavas, defining parallel arrays in $^{206}Pb/^{204}Pb$–$^{207}Pb/^{204}Pb$ space (Figs. 3c and 6a). While the HIMU lavas from the Austral Islands plot on the northern hemisphere reference line (NHRL; Hart, 1984), those from St. Helena plot above this line. The least-square regressions for the St. Helena and Austral Islands arrays do not converge, which suggests the absence of common mixing components in the radiogenic and the unradiogenic ends (see caption of Fig. 6). Consequently, both the depleted component and the HIMU component for St. Helena should have elevated $^{207}Pb/^{204}Pb$ relative to those for Austral Islands. Since high $^{206}Pb/^{204}Pb$ in the HIMU component require long-term evolution of Pb isotopes, the elevation in $^{207}Pb/^{204}Pb$ should also reflect ancient (>1.5 Ga) processes that fractionated U/Pb (Vidal, 1992; Chauvel et al., 1992, 1995; Thirlwall, 1997), as discussed in detail in the next section. On the other hand, provided that the linear trends in Pb isotope spaces were ascribed to recent mixing of the HIMU component from an upwelling plume with the ambient depleted mantle, the elevated $^{207}Pb/^{204}Pb$ relative to NHRL in the depleted component would be the feature of the local mantle beneath St. Helena.

A likely explanation for the isotopically different depleted components beneath St. Helena and Austral Islands is global heterogeneity in the Atlantic and Pacific upper mantle. The isotopic composition of the upper mantle is approximated by N-MORB that erupt away from areas of plume–ridge interactions. Pacific MORB define a narrow array overlapping with NHRL, whereas Atlantic MORB show variously elevated $^{207}Pb/^{204}Pb$ relative to NHRL (Fig. 6a). The elevated $^{207}Pb/^{204}Pb$ becomes more prominent, in combination with decreasing $^{176}Hf/^{177}Hf$, from north to south along the mid-Atlantic ridge (Andres

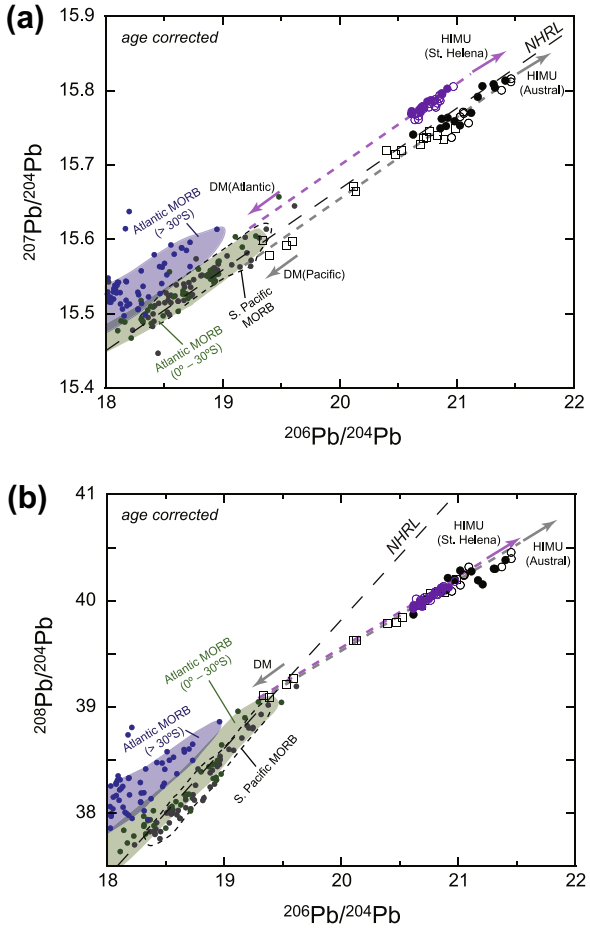

Fig. 6. Age-corrected Pb isotopic compositions of the St. Helena and Austral Islands HIMU lavas. Large solid and open circles denote whole-rocks and clinopyroxene separates from subaerial lavas. Open squares represent submarine lavas from Austral Islands. (a) Lavas from St. Helena (purple symbols) and Austral Islands (black symbols) define parallel trends. The regression lines for St. Helena (pink dashed line) and Austral Islands (gray dashed line) were calculated by using age-corrected whole-rock Pb isotope ratios as; $(^{207}Pb/^{204}Pb) = 0.109 \times (^{206}Pb/^{204}Pb) + 13.52$ ($n = 25$) and $(^{207}Pb/^{204}Pb) = 0.109 \times (^{206}Pb/^{204}Pb) + 13.47$ ($n = 22$), respectively. (b) Lavas from St. Helena (purple symbols) and Austral Islands (black symbols) define overlapping trends. The regression lines for St. Helena and Austral Islands are; $(^{208}Pb/^{204}Pb) = 0.656 \times (^{206}Pb/^{204}Pb) + 26.43$ and $(^{208}Pb/^{204}Pb) = 0.646 \times (^{206}Pb/^{204}Pb) + 26.60$, respectively. The isotopic data and their typical isotopic range for south Atlantic MORB (green: 0–30°S; blue: >30°S) and south Pacific MORB (gray dots and fields surrounded by the dashed lines) are shown as potential mixing components for the St. Helena and Austral Islands lavas, respectively. Data sources are White et al. (1987), Hanan and Schilling (1989), Haase (2002), and Agranier et al. (2005). The age-corrected Pb isotope ratios for the HIMU lavas are from Hanyu et al. (2011a, 2013) and this study. (For interpretation of the references to color in this figure legend, the reader is referred to the web version of this article.)

et al., 2004). Indeed, the Atlantic N-MORB in the interval between 0° and 30°S near St. Helena do not show significant elevation in $^{207}Pb/^{204}Pb$ from NHRL as a group. However, the presence of a few N-MORB with elevated $^{207}Pb/^{204}Pb$ in this section (Agranier et al., 2005) implies existence of the high-$^{207}Pb/^{204}Pb$ material in the upper mantle near St. Helena. Andres et al. (2004) attributed the along-ridge $^{207}Pb/^{204}Pb$ and $^{176}Hf/^{177}Hf$ variations to the entrainment of continental restite in the upper mantle during the opening of the Atlantic. The mid-Atlantic ridge near St. Helena would be the transient region, where the proportion of continental restite in the upper mantle increases toward the south (>30°S). This may explain the radiogenic ^{207}Pb in the ambient depleted mantle beneath St. Helena.

5.4. $^{207}Pb/^{204}Pb$; formation ages of the HIMU reservoirs

The HIMU lavas from St. Helena and Austral Islands share most radiogenic Pb isotopic feature among OIB, but St. Helena HIMU lavas show higher $^{207}Pb/^{204}Pb$ for a given $^{206}Pb/^{204}Pb$ than the Austral HIMU lavas. Radiogenic Pb isotopic compositions require ancient fractionations of U/Pb and Th/Pb in the HIMU components. In particular, the combination of $^{206}Pb/^{204}Pb$ and $^{207}Pb/^{204}Pb$ provides information for the reservoir formation age because both ratios evolve coherently depending on μ in the component (Zindler and Hart, 1986; Vidal, 1992; Hauri and Hart, 1993; Thirlwall, 1997). Therefore, the difference in the $^{206}Pb/^{204}Pb$ and $^{207}Pb/^{204}Pb$ systematics between the HIMU lavas for St. Helena and Austral Islands would reflect different formation ages of the two HIMU components, if they derived from materials with similar Pb isotopic evolution.

To model the Pb isotope evolution in the HIMU components, we assume that the HIMU precursor was ancient subducted oceanic crust or lithospheric mantle which was chemically modified at the time, T_{HIMU}, and that it had the same Pb isotope ratios with the depleted upper mantle at T_{HIMU}. For the latter assumption, we use the upper mantle Pb isotope evolution model of Elliott et al. (1999) because their model solves the so-called "κ-conundrum", an apparent decoupling of κ ($=^{232}Th/^{238}U$) independently determined by $^{208}Pb/^{206}Pb$ and Th/U in MORB (Galer and O'Nions, 1985). μ and κ in the depleted upper mantle change with time as shown in the insets in Fig. 7(a and b) (μ and κ are corrected for decay to present-day). The concept of monotonous change in μ and κ since Archean (2.5 or 3.5 Ga) is based on the selective recycling of U back to the mantle in the post-Archean era, as discussed in detail below (Elliott et al., 1999; Collerson and Kamber, 1999; Nielsen, 2010). The Pb isotope evolution is calculated with given variables; onset time of Pb isotope evolution in the silicate Earth (4.53–4.56 Ga), initial μ-value (7.8–8.2), and onset time of μ and κ change in the depleted mantle (2.5–3.5 Ga) (Table A5 in Appendix). The Pb isotope ratios in the HIMU component evolved from T_{HIMU} to the present with constant μ_{HIMU} and κ_{HIMU} (see Appendix for the detailed description for the model).

Fig. 7a shows the present-day $^{206}Pb/^{204}Pb$ and $^{207}Pb/^{204}Pb$ of the HIMU component as functions of μ_{HIMU} and T_{HIMU} with fixed variables as a standard case (see the caption for the variables chosen). Since the HIMU components for St. Helena and Austral Islands should have

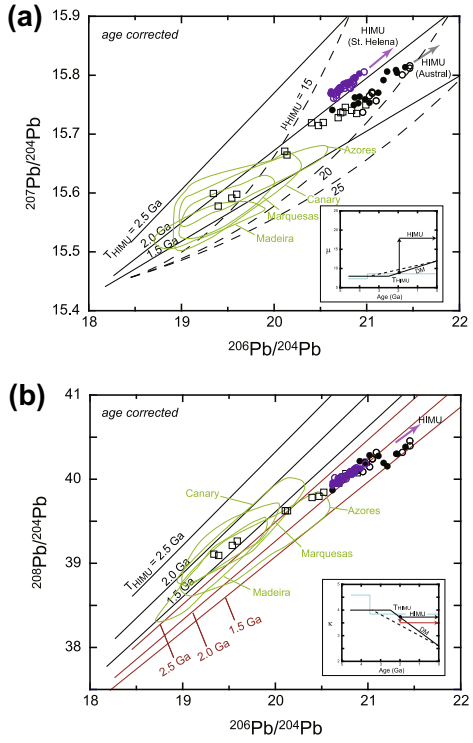

Fig. 7. Calculated Pb isotopic compositions of the present-day HIMU component. Insets schematically show the μ and κ evolution of the depleted upper mantle (DM) and HIMU component in the model. In DM, μ and κ (corrected for decay to present-day) were constant from the beginning of the silicate Earth, and then changed linearly to the present values since 2.5 Ga (black solid lines) or 3.5 Ga (dashed lines). The two-stage μ and κ evolution model by Stacey and Kramers (1975) are also shown for comparison (light blue lines). The altered oceanic crust, that is the HIMU precursor, formed from the depleted upper mantle at T_{HIMU}, and μ_{HIMU} increased from μ_{DM} since then (inset in (a)). κ_{HIMU} was either unchanged or modified from κ_{DM} at T_{HIMU} (black and red arrows in inset in (b)). The main panels show the present-day $^{206}Pb/^{204}Pb$, $^{207}Pb/^{204}Pb$ and $^{208}Pb/^{204}Pb$ of the HIMU component as functions of μ_{HIMU} and T_{HIMU} using the following variables as a standard case; 4.55 Ga for the onset time of Pb isotope evolution, 8.0 for the initial μ-value, and 2.5 Ga for the onset time of μ and κ change in the depleted mantle (Table A5 in Appendix). The solid lines in (a) indicate isopleths for fixed T_{HIMU} (=1.5, 2.0, and 2.5 Ga) with different μ_{HIMU}. The dashed lines indicate isopleths for fixed μ_{HIMU} (=15, 20, and 25) with different T_{HIMU}. The ages of the HIMU reservoirs for St. Helena and Austral Islands are constrained around 2 Ga because the mixing trends are subparallel to the 2.0 Ga isopleth. In (b), the 2.0 Ga isopleth does not overlap with the $^{206}Pb/^{204}Pb$ and $^{208}Pb/^{204}Pb$ of the HIMU lavas if Th/U did not fractionate during the formation of oceanic crust (i.e., $\kappa_{HIMU} = \kappa_{DM}$ at T_{HIMU}; black lines). This mismatch is reconciled by assuming 13% reduction of κ_{HIMU} from κ_{DM} (note that $\kappa_{DM} = 4.0$, 3.7, and 3.4 at $T_{HIMU} = 2.5$, 2.0, and 1.5 Ga, respectively) during the formation of altered oceanic crust (red lines). The fields surrounded by green lines indicate the isotopic range of young-HIMU lavas from Marquesas, Canary, Azores, and Madeira (Dupuy et al., 1987; Vidal, 1992; Thirlwall, 1997; Geldmacher and Hoernle, 2000; Millet et al., 2008; Day et al., 2010; compiled data from Stracke (2012)). (For interpretation of the references to color in this figure legend, the reader is referred to the web version of this article.)

more radiogenic Pb isotopes than any observed lavas, μ_{HIMU} is higher than 17 in this case. T_{HIMU} can be also constrained from the $^{206}Pb/^{204}Pb$–$^{207}Pb/^{204}Pb$ diagram. We noted above that the linear arrays defined by the St. Helena and Austral Islands lavas are not isochrons, but mixing trends; thereby the slope of the trends does not directly relate with the reservoir formation age. However, on the grounds that the two HIMU components should plot on the extensions of the mixing trends defined by each lava suite, and that the trends are nearly parallel to the 2 Ga isopleth, T_{HIMU} is likely to be around 2 Ga (Fig. 7a). In detail, calculated T_{HIMU} for St. Helena and Austral Islands varies from 1.8 to 2.3 Ga and from 1.5 to 2.0 Ga, respectively, when adopting the range of variables in the model (Table A5 in Appendix). T_{HIMU} in this model is consistent with the previous estimates employing single-stage or two-stage Pb evolution model in the mantle (e.g., Chauvel et al., 1992; Hauri and Hart, 1993; Stracke et al., 2003) on account of similar μ assumed in the early half of the mantle evolution (inset in Fig. 7a).

An important implication from this model is that the HIMU component for St. Helena is older than that for Austral Islands. Fig. 7a illustrates that the age difference between the two HIMU components is approximately 0.3 Ga, and this significance remains even if different variables are adopted in the model calculation (Table A5 in Appendix). We emphasize that the HIMU reservoir for St. Helena could form earlier than that for Austral Islands by ~0.3 Ga.

In reality, the meaning of the reservoir formation age (T_{HIMU}) is obscured by the nature of the HIMU reservoirs. If mantle plumes sample a small-scale reservoir that was formed at a certain time and remained isolated since then, the formation age of the reservoir, more precisely component in this case, can be clearly defined. In contrast, if the HIMU reservoir was a large-scale reservoir formed by the continuous accumulation of ancient subducted oceanic crust and lithospheric mantle at some period, then the calculated T_{HIMU} indicates the integrated age of the subducted material in terms of Pb. In the second case, the HIMU reservoir for St. Helena should involve greater amounts of older subducted material than that for Austral Islands.

Considering that the HIMU components for St. Helena and Austral Islands have very similar Sr, Nd, Hf, $^{206}Pb/^{204}Pb$, and $^{208}Pb/^{204}Pb$ isotopic compositions, the first model seems less likely because either the subducted oceanic crust or lithospheric mantle that were chemically modified prior to subduction should have potential compositional heterogeneity (Stracke et al., 2003; Pilet et al., 2005). Therefore, the subducted material produced at different ages and places would not have similar isotopic compositions after time. In the long-term accumulation model, geochemically heterogeneous subducted materials could be mechanically stirred and their compositions could be averaged during the accumulation process, resulting in forming large-scale HIMU reservoirs in the deep mantle (Nakagawa and Tackley, 2005; McNamara et al., 2010). Moreover, partial melting of subducted materials and subsequent hybridization with ambient mantle may facilitate the formation of geochemically homogeneous HIMU reservoirs (Hanyu et al., 2011a).

If the HIMU reservoirs formed by continuous accumulation of ancient subducted oceanic crust and lithosphere at some period, there should be other HIMU reservoirs that show younger integrated Pb isotope age than the HIMU reservoirs for St. Helena and Austral Islands. The presence of "young-HIMU" component has been advocated in OIB at Canary, Azores, Madeira, and Maquesas Islands (Dupuy et al., 1987; Vidal, 1992; Thirlwall, 1997; Geldmacher and Hoernle, 2000; Millet et al., 2008; Day et al., 2010). These lavas are characterized by unradiogenic $^{87}Sr/^{86}Sr$ and selective depletion in fluid-mobile elements that are common to the HIMU lavas from St. Helena and Austral Islands. However, Pb isotopes of these lavas are less radiogenic ($^{206}Pb/^{204}Pb < 20.5$), and more importantly, $^{207}Pb/^{204}Pb$ are lower at a given $^{206}Pb/^{204}Pb$ relative to NHRL unlike those from St. Helena and Austral Islands (Fig. 7a). Such $^{206}Pb/^{204}Pb$–$^{207}Pb/^{204}Pb$ systematics can be interpreted as that the HIMU reservoirs for Canary, Azores, Madeira, and Marquesas Islands involve young subducted materials more abundant than those for St. Helena and Austral Islands. The HIMU reservoirs containing subducted material with various ages would exist ubiquitously in the mantle (Christensen and Hofmann, 1994; Stracke et al., 2005; Brandenburg et al., 2008).

5.5. $^{208}Pb/^{204}Pb$; fractionation of Th/U in the ancient Earth

The $^{206}Pb/^{204}Pb$–$^{208}Pb/^{204}Pb$ systematics constrain the time-integrated Th/U ratio (κ) in the HIMU components. Chauvel et al. (1992) documented that the time-integrated κ of the HIMU lavas from Tubuai in the Austral Islands is about 3.7. This value is close to but slightly lower than the bulk Earth κ value of about 4. The Pb isotope evolution model used in this study also suggests similar κ_{HIMU}. Fig. 7b (black lines) shows the isopleths for a given T_{HIMU} by assuming $\kappa_{HIMU} = \kappa_{DM}$ at T_{HIMU} (see inset of Fig. 7b). The St. Helena and Austral Islands lavas plot below the 2 Ga and even 1.5 Ga isopleths, displaying an apparent discrepancy between the $^{206}Pb/^{204}Pb$–$^{207}Pb/^{204}Pb$ and $^{206}Pb/^{204}Pb$–$^{208}Pb/^{204}Pb$ systematics (Fig. 7).

This discrepancy is reconciled by reducing the κ_{HIMU} value by only 10–15% relative to κ_{DM} at T_{HIMU} in the case when the onset time of μ and κ change in the depleted mantle is 2.5 Ga (red lines in Fig. 7b). If we adopt the onset time of μ and κ change in the depleted mantle of 3.5 Ga in the calculation, the discrepancy is almost disappeared (i.e., $\kappa_{HIMU}/\kappa_{DM}$ at $T_{HIMU} \sim 1$; Table A5 in Appendix). Similarly, modification of κ_{HIMU} from κ_{DM} is not necessary by assuming slightly lower initial κ_{DM} of 3.6–3.8 instead of a fixed initial κ_{DM} value of 4 used in the model calculation. This approach suggests that the required κ_{HIMU} for both St. Helena and Austral Islands HIMU components is 3.3–3.7. Stracke et al. (2003) also obtained similar κ_{HIMU} with their single-stage mantle Pb evolution model.

The estimated κ_{HIMU} is higher than the present-day κ_{DM}. Stracke et al. (2003) compiled the trace element composition of N-MORB and showed that despite the significant variation in Th/U ($\sim 0.97 \times \kappa$) around the arithmetic average value of $\kappa = 2.6$, N-MORB with $\kappa > 3.3$ are minor. This appears contradictory to the model that the HIMU component formed from subducted oceanic crust (Stracke et al., 2003). However, a potential mismatch between κ_{HIMU} and present-day κ_{DM} may be reconciled by considering the fact that the average Th/U of global MORB determined by the recent high-precision analyses of fresh MORB glasses has been revised to higher value of 2.9 (Arevalo and McDonough, 2010) and 3.1 (Gale et al., 2013), and therefore the population of N-MORB with $\kappa > 3.3$ is larger than previously thought. More importantly, the ancient depleted upper mantle, and hence the ancient subducted oceanic crust, had higher κ than the modern equivalents owing to the monotonous decrease in Th/U in the upper mantle in the post-Archean (Elliott et al., 1999). Such temporal evolution in Th/U in the depleted upper mantle has been documented in ancient MORB and komatiites, which record constant Th/U close to the chondritic ratio in the Archean and declining Th/U from the late Archean or early Proterozoic to the present (Collerson and Kamber, 1999; Nakamura and Kato, 2007; Nielsen, 2010).

However, another problem arises in terms of Th/U if the precursor of the HIMU reservoir involved altered basaltic layers in the oceanic crust. Th and U are equally incompatible during mantle melting, and therefore, the generated oceanic crust can have the same Th/U with the upper mantle. Hydrothermal alteration near mid-ocean ridges enriches oceanic crust in terms of U relative to Th, as typically observed in modern carbonated altered oceanic crust because oxidized U is much more fluid-soluble than Th (Staudigel et al., 1996; Bach et al., 2003; Kelley et al., 2003). Therefore, the present-day manner of hydrothermal activity with oxic fluids may give rise to drastic lowering of Th/U in the altered oceanic crust.

Bach et al. (2003) estimated by the study of drilled cores at Sites 504B and 417/418 that the altered basaltic layer in the upper crust gained μ of 17–33 and κ of 0.2–2.1. The μ range is sufficiently high for radiogenic $^{206}Pb/^{204}Pb$ and $^{207}Pb/^{204}Pb$, whereas κ is too low and accordingly Th/Pb ($\sim \mu \times \kappa$) is not high enough to evolve $^{208}Pb/^{204}Pb$ in 2 Ga required for the HIMU reservoir (Bach et al., 2003). The problem of low-κ cannot be reconciled if bulk oceanic crust is considered as the HIMU precursor because U is highly concentrated in the uppermost altered basaltic layer compared to the unaltered sheeted dykes and gabbroic layers in the middle and lower oceanic crust (Stracke et al., 2003). Bach et al. (2003) suggested that removal of 80–90% Pb, 35–40% U, and 0% Th from altered oceanic crust is required during subduction dehydration to account for the Pb isotopic compositions of the HIMU component. However, the high-pressure experiments documented that U and Th are less soluble to fluids, and therefore the increase in κ is small during dehydration of the subducted oceanic crust (Kogiso et al., 1997a). A solution to the low-κ problem may be that the HIMU precursor involved only unaltered and unhydrated parts of oceanic crust, although this theory does not account for depletion in fluid-mobile elements in the HIMU lavas. Moreover, it seems unlikely that the upper altered basalt layer that is several hundred meters thick had been selectively stripped off from the subducted oceanic crust.

Alternative model is that the HIMU precursor was an oceanic crust hydrothermally altered in the anoxic marine environment before the Great Oxidation Event (GOE; Kasting, 1993; Holland, 2006). Under the anoxic conditions, reduced U and Th behaved similarly and were insoluble to the seawater. The uptake of U and Th from seawater was limited, or if any, Th/U was not fractionated during low-temperature alteration or hydrothermal alteration of the oceanic crust in such environment (Nakamura and Kato, 2007). Consequently, the hydrothermal alteration would not lower Th/U in the subducted oceanic crust before the GOE.

This model is consistent with the theory that accounts for the temporal evolution in Th/U in the depleted upper mantle mentioned above (Collerson and Kamber, 1999; Nielsen, 2010). These authors suggested that chondritic κ was maintained in the Archean mantle because of limited transport of U and Th from hydrosphere to the mantle by subduction of oceanic crust before the GOE. The onset of the Th/U decrease in the upper mantle is related with the enhanced weathering transport of U from continental crust to the ocean coupled with formation of U-rich hydrothermally altered oceanic crust in response to the increasing oxygen levels in the hydrosphere. Subduction of such altered oceanic crust with low Th/U would promote the continuous decrease in Th/U in the upper mantle after the GOE (Collerson and Kamber, 1999; Nielsen, 2010).

The formation age of the HIMU reservoirs deduced from U–Th–Pb systematics leaves some uncertainties depending on the model assumptions for the Pb isotopic evolution in the depleted mantle (1.5–2.3 Ga). However, all the age estimates for the HIMU reservoir postdates the GOE at 2.45 Ga (Holland, 2006) (Fig. 8). This age gap might reflect the delay of the oxygen level increase in the deep seawater (1.85 Ga) relative to that in the shallow seawater and the atmosphere (Kasting, 1993; Holland, 2006). On the other hand, the recent discovery of mass-independent fractionation of sulfur isotopes in the Mangaia lavas in Austral Islands suggests that the formation of the HIMU reservoir predates the GOE (Cabral et al., 2013). Because subduction input has been a continuous process through the Earth's history, the HIMU reservoir, in reality, would have formed by the long-term accumulation of subducted altered oceanic crust over a certain period around the GOE. The validity of this model can be tested in the future whether the mass-independent fractionation of sulfur isotopes is observed in the St. Helena lavas, because Pb isotope systematics suggest older formation age of the HIMU reservoir for St. Helena than that for Austral Islands.

The $^{206}Pb/^{204}Pb$–$^{208}Pb/^{204}Pb$ systematics of the young-HIMU lavas imply their κ values as high as those of the St. Helena and Austral Islands lavas (Fig. 7b). However, it is expected that the young altered oceanic crust would have low Th/U due to hydrothermal alteration with oxic fluids, and thereby the young-HIMU components should have low κ. A possible explanation for high κ in the young-HIMU components may be recycling of young subducted materials with increased Th/U due to extensive U removal when dehydration predominates the subduction modification processes in response to secular mantle cooling (Vidal, 1992). Another possibility is that the young-HIMU reservoirs also formed by long-term accumulation of subducted materials with younger integrated age than the HIMU reservoirs for St. Helena and Austral Islands. If the young-HIMU reservoirs contain significant amount of oceanic crust altered with anoxic deep water before 1.85 Ga, it could maintain high Th/U. The model depends on when the oxic conditions started in the deep marine environment and how young the young-HIMU reservoirs are.

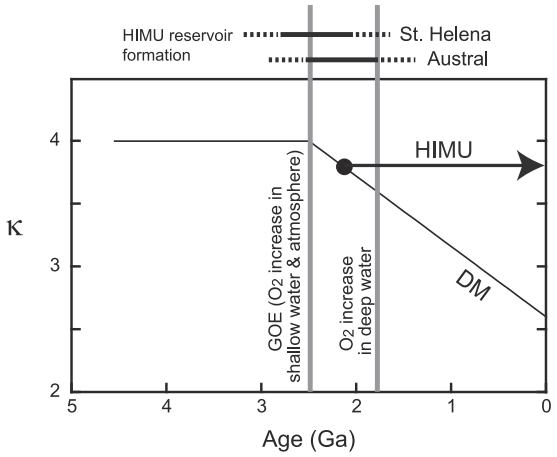

Fig. 8. Schematic of the κ evolution in the depleted mantle and the HIMU reservoir. The κ_{DM} decrease is triggered by the onset of the recycling of U from the hydrosphere to the mantle through subducted oceanic crust that scavenges oxidized U from seawater after the GOE at 2.45 Ga (Elliott et al., 1999). However, because oxidization is delayed until 1.85 Ga in the deep marine environment (Holland, 2006), some oceanic crust did not scavenge U effectively and therefore, did not have very low Th/U by hydrothermal alteration (see Section 5.5). The fact that the Pb isotope ages are younger than 2.3 Ga, that the HIMU precursor should not have low Th/U like modern altered oceanic crust, and that the HIMU component possesses mass-independent fractionated sulfur isotopes (Cabral et al., 2013) is best explained by accumulation of oceanic crust created before and after the GOE, and they are homogenized in the HIMU reservoir. Because the Pb isotope age for St. Helena is older than that for Austral Islands by 0.3 Ga (see Section 5.4), the HIMU reservoir for St. Helena involved old subducted material more abundant than that for Austral Islands.

6. CONCLUDING REMARKS

The lavas exposed on St. Helena show isotopic variations between the volcanic stages in the NE and SW volcanoes. The isotopic variations are regarded as the change of the mixing fractions of melts from the HIMU component against the depleted component in the ambient mantle. The mixing arrays defined by the St. Helena lavas are remarkably similar to those observed in HIMU lavas from the Austral Islands in the South Pacific in terms of $^{87}Sr/^{86}Sr$, $^{143}Nd/^{144}Nd$, $^{176}Hf/^{177}Hf$, $^{206}Pb/^{204}Pb$, and $^{208}Pb/^{204}Pb$. These isotopic evidences are consistent with the model that the HIMU precursor is ancient subducted oceanic crust and lithosphere. However, there is a significant difference between the HIMU lavas from St. Helena and Austral Islands in $^{207}Pb/^{204}Pb$.

The formation ages of the St. Helena and Austral Islands HIMU reservoirs were evaluated using Pb isotope systematics. Model calculations using $^{206}Pb/^{204}Pb$–$^{207}Pb/^{204}Pb$ systematics and the depleted mantle Pb evolution model of Elliott et al. (1999) demonstrated that the HIMU reservoirs formed around 2 Ga. More importantly, the HIMU reservoir for St. Helena is older than that for Austral Islands by ~0.3 Ga. We interpret the age difference as that the HIMU reservoir for St. Helena involved old subducted materials more abundant than that for Austral Islands during the long-term accumulation of subducted materials. The isotopic similarity between the two HIMU reservoirs requires homogenization of intrinsically heterogeneous subducted oceanic crust.

The κ values of the HIMU components determined by the $^{206}Pb/^{204}Pb$–$^{208}Pb/^{204}Pb$ evolution model are distinctly higher than the κ from the present-day hydrothermally altered oceanic crust. This apparently contradicts the model that the HIMU precursor is subducted altered oceanic crust because Th/U is highly modified by U-rich hydrothermal fluids under oxic marine conditions. The effect of the hydrothermal alteration of oceanic crust was presumably different between ancient and present times; the anoxic marine environment prevented the uptake of U by the altered oceanic crust via hydrothermal fluids when the HIMU precursor was formed. In this scenario, the depleted upper mantle maintained a chondritic κ value in the Archean even if the input of subducted oceanic crust took place since the early stages of mantle evolution. The post-Archean monotonous decrease in κ to the present mantle value would be caused by the change in the recycling of U induced by surface oxidation. The formation age of ~2 Ga and the high-κ value of the HIMU reservoir provide a coherent interpretation of the growth history of κ in the depleted upper mantle.

ACKNOWLEDGMENTS

This paper owes much to the help by Ian Baker, who has been studying of St. Helena for more than 40 years, during our field trip on the island. Thanks go to the staff of the Kyoto Fission-Track Co. Ltd. for their effort for preparing pure mineral separates. Also we thank B.S. Vaglarov for his help with the isotope analyses. We are grateful to the staff of the Japan Research Reactor No. 3 (JRR3) of the Japan Atomic Energy Agency for the neutron irradiation of the samples for laser fusion Ar–Ar dating. Careful reviews by C. Chauvel, J. Day, an anonymous reviewer, and the associate editor A. Stracke have greatly improved the manuscript.

APPENDIX A. SUPPLEMENTARY DATA

Supplementary data associated with this article can be found, in the online version, at http://dx.doi.org/10.1016/j.gca.2014.03.016.

REFERENCES

Abdel-Monem A. and Gast P. W. (1967) Age of volcanism on St. Helena. *Earth Planet. Sci. Lett.* **2**, 415–418.

Agranier A., Blichert-Toft J., Graham D., Debaille V., Schiano P. and Albarède F. (2005) The spectra of isotopic heterogeneities along the mid-Atlantic ridge. *Earth Planet. Sci. Lett.* **238**, 96–109.

Andres M., Blichert-Toft J. and Schilling J. G. (2004) Nature of the depleted upper mantle beneath the Atlantic: evidence from Hf isotopes in normal mid-ocean ridge basalts from 79 degrees N to 55 degrees S. *Earth Planet. Sci. Lett.* **225**, 89–103.

Arevalo, Jr, R. and McDonough W. F. (2010) Chemical variations and regional diversity observed in MORB. *Chem. Geol.* **271**, 70–85.

Bach W., Alt J. C., Niu Y., Humphris S. E., Erzinger J. and Dick H. J. B. (2001) The geochemical consequences of late-stage low-grade alteration of lower ocean crust at the SW Indian ridge: results from ODP Hole 735B (Leg 176). *Geochim. Cosmochim. Acta* **65**, 3267–3287.

Bach W., Peucker-Ehrenbrink B., Hart S. R. and Blusztajn J. S. (2003) Geochemistry of hydrothermally altered oceanic crust: DSDP/ODP Hole 504B – implications for seawater–crust exchange budgets and Sr- and Pb-isotopic evolution of the mantle. *Geochem. Geophys. Geosyst.* **4**, 8904.

Baker I. (1969) Petrology of the volcanic rocks of Saint Helena Island, South Atlantic. *Geol. Soc. Am. Bull.* **80**, 1283–1310.

Baker I., Gale N. H. and Simons J. (1967) Geochronology of the St. Helena volcanoes. *Nature* **215**, 1451–1456.

Baker J., Peate D., Waight T. and Meyzen C. (2004) Pb isotope analysis of standards and samples using ^{207}Pb–^{204}Pb double spike and thallium to correct for mass bias with a double-focusing MC-ICP-MS. *Chem. Geol.* **211**, 275–303.

Baksi A. K. (2003) Critical evaluation of $^{40}Ar/^{39}Ar$ ages for the Central Atlantic Magmatic Province: timing, duration and possible migration of magmatic centers. In *The Central Atlantic Magmatic Province: Insights from Fragments of Pangea* (eds. W. Harmes, J. G. McHone, P. Renne and C. Ruppel). AGU, Washington, D.C., pp. 77–90.

Becker H., Jochum K. P. and Carlson R. W. (2000) Trace element fractionation during dehydration of eclogites from high-pressure terranes and the implications for element fluxes in subduction zones. *Chem. Geol.* **163**, 65–99.

Brandenburg J. P., Hauri E. H., van Keken P. E. and Ballentine C. J. (2008) A multiple-system study of the geochemical evolution of the mantle with force-balanced plates and thermochemical effects. *Earth Planet. Sci. Lett.* **276**, 1–13.

Cabral R. A., Jackson M. G., Rose-Koga E. F., Koga K. T., Whitehouse M. J., Antonelli M. A., Farquhar J., Day J. M. D. and Hauri E. H. (2013) Anomalous sulphur isotopes in plume lavas reveal deep mantle storage of Archaean crust. *Nature* **496**, 490–493.

Chaffey D. J., Cliff R. A. and Wilson B. M. (1989) Characterization of the St Helena magma source. In *Magmatism in the Ocean Basins* (eds. A. D. Saunders and M. J. Norry). Geological Society Special Publication, pp. 257–276.

Chang Q., Shibata T., Sinotsuka K., Yoshikawa M. and Tatsumi Y. (2003) Precise determination of trace elements in geological standard rocks using inductively coupled plasma mass spectrometry (ICP-MS). *Frontier Research on Earth Evolution 1. IFREE Report for* **2001–2002**, 357–362.

Chauvel C., Hofmann A. W. and Vidal P. (1992) HIMU-EM: The French Polynesian connection. *Earth Planet. Sci. Lett.* **110**, 99–119.

Chauvel C., Goldstein S. L. and Hofmann A. W. (1995) Hydration and dehydration of oceanic-crust controls Pb evolution in the mantle. *Chem. Geol.* **126**, 65–75.

Chauvel C., Lewin E., Carpentier M., Arndt N. T. and Marini J.-C. (2008) Role of recycled oceanic basalt and sediment in generating the Hf–Nd mantle array. *Nat. Geosci.* **1**, 64–67.

Christensen U. R. and Hofmann A. W. (1994) Segregation of subducted oceanic-crust in the convecting mantle. *J. Geophys. Res.* **99**, 19867–19884.

Collerson K. D. and Kamber B. S. (1999) Evolution of the continents and the atmosphere inferred from Th–U–Nb systematics of the depleted mantle. *Science* **283**, 1519–1522.

Day J. M. D. and Hilton D. R. (2011) Origin of $^{3}He/^{4}He$ ratios in HIMU-type basalts constrained from Canary Island lavas. *Earth Planet. Sci. Lett.* **305**, 226–234.

Day J. M. D., Pearson D. G., Macpherson C. G., Lowry D. and Carracedo J. C. (2010) Evidence for distinct proportions of subducted oceanic crust and lithosphere in HIMU-type mantle beneath El Hierro and La Palma. *Canary Islands. Geochim. Cosmochim. Acta* **74**, 6565–6589.

Dupré B., Lambret B. and Allègre C. J. (1982) Isotopic variations within a single oceanic island: the Terceira case. *Nature* **299**, 620–622.

Dupuy C., Vidal P., Barsczus H. G. and Chauvel C. (1987) Origin of basalts from the Marquesas Archipelago (south central Pacific Ocean): isotope and trace element constraints. *Earth Planet. Sci. Lett.* **82**, 145–152.

Dupuy C., Barsczus H. G., Liotard J. M. and Dostal J. (1988) Trace element evidence for the origin of ocean island basalts: an example from the Austral Islands (French Polynesia). *Contrib. Mineral. Petrol.* **98**, 293–302.

Eisele J., Sharma M., Galer S. J. G., Blichert-Toft J., Devey C. W. and Hofmann A. W. (2002) The role of sediment recycling in EM-1 inferred from Os, Pb, Hf, Nd, Sr isotope and trace element systematics of the Pitcairn hotspot. *Earth Planet. Sci. Lett.* **196**, 197–212.

Elliott T., Zindler A. and Bourdon B. (1999) Exploring the kappa conundrum: the role of recycling in the lead isotope evolution of the mantle. *Earth Planet. Sci. Lett.* **169**, 129–145.

Gale A., Dalton C. A., Langmuir C. H., Su Y. and Schilling J.-G. (2013) The mean composition of ocean ridge basalts. *Geochem. Geophys. Geosyst.* **14**, 489–518.

Galer S. J. G. and O'Nions K. (1985) Residence time of thorium, uranium and lead in the mantle with implications for mantle convection. *Nature* **316**, 778–782.

Geldmacher J. and Hoernle K. (2000) The 72 Ma geochemical evolution of the Madeira hotspot (eastern North Atlantic): recycling of Paleozoic ($\leqslant$500 Ma) oceanic lithosphere. *Earth Planet. Sci. Lett.* **183**, 73–92.

Graham D. W., Humphris S. E., Jenkins W. J. and Kurz M. D. (1992) Helium isotope geochemistry of some volcanic rocks from Saint Helena. *Earth Planet. Sci. Lett.* **110**, 121–131.

Haase K. M. (2002) Geochemical constraints on magma sources and mixing processes in Easter Microplate MORB (SE Pacific): a case study of plume–ridge interaction. *Chem. Geol.* **182**, 335–355.

Hanan B. B. and Schilling J.-G. (1989) Easter microplate evolution: Pb isotope evidence. *Journal of Geophysical Research: Solid Earth* **94**, 7432–7448.

Hanyu T. and Kaneoka I. (1997) The uniform and low $^{3}He/^{4}He$ ratios of HIMU basalts as evidence for their origin as recycled materials. *Nature* **390**, 273–276.

Hanyu T. and Nakamura E. (2000) Constraints on HIMU and EM by Sr and Nd isotopes re-examined. *Earth Planets Space* **52**, 61–70.

Hanyu T., Tatsumi Y. and Kimura J.-I. (2011a) Constraints on the origin of the HIMU reservoir from He–Ne–Ar isotope systematics. *Earth Planet. Sci. Lett.* **307**, 377–386.

Hanyu T., Tatsumi Y., Senda R., Miyazaki T., Chang Q., Hirahara Y., Takahashi T., Kawabata H., Suzuki K. and Kimura J.-I. (2011b) Geochemical characteristics and origin of the HIMU reservoir: a possible mantle plume source in the lower mantle. *Geochem. Geophys. Geosyst.* **12**, Q0AC09.

Hanyu T., Dosso L., Ishizuka O., Tani K., Hanan B. B., Adam C., Nakai S., Senda R., Chang Q. and Tatsumi Y. (2013) Geochemical diversity in submarine HIMU basalts from Austral Islands, French Polynesia. *Contrib. Mineral. Petrol.* **166**, 1285–1304.

Hart S. R. (1984) A large-scale isotope anomaly in the Southern Hemisphere mantle. *Nature* **309**, 753–757.

Hauri E. H. and Hart S. R. (1993) Re-Os isotope systematics of HIMU and EMII oceanic island basalts from the south Pacific Ocean. *Earth Planet. Sci. Lett.* **114**, 353–371.

Hémond C., Devey C. W. and Chauvel C. (1994) Source compositions and melting processes in the Society and Austral plumes (South Pacific Ocean): element and isotope (Sr, Nd, Pb, Th) geochemistry. *Chem. Geol.* **115**, 7–45.

Hirahara Y., Takahashi T., Miyazaki T., Vaglarov B. S., Chang Q., Kimura J.-I. and Tatsumi Y. (2009) Precise Nd isotope analysis of igneous rocks using cation exchange chromatography and thermal ionization mass spectrometry (TIMS). *JAMSTEC Rep. Res. Develop. Spec. Issue*, 65–71.

Hofmann A. W. (1997) Mantle geochemistry: the message from oceanic volcanism. *Nature* **385**, 219–229.

Hofmann A. W. and White W. M. (1982) Mantle plumes from ancient oceanic crust. *Earth Planet. Sci. Lett.* **57**, 421–436.

Holland H. D. (2006) The oxygenation of the atmosphere and oceans. *Philos. Trans. R. Soc. B* **361**, 903–915.

Hyodo H. (2008) Laser probe $^{40}Ar/^{39}Ar$ dating: history and development from a technical perspective. *Gond. Res.* **14**, 609–616.

Ito G. and Mahoney J. J. (2005) Flow and melting of a heterogeneous mantle: 1. Method and importance to the geochemistry of ocean island and mid-ocean ridge basalts. *Earth Planet. Sci. Lett.* **230**, 29–46.

Jackson M. G., Hart S. R., Koppers A. A. P., Staudigel H., Konter J., Blusztajn J., Kurz M. and Russell J. A. (2007) The return of subducted continental crust in Samoan lavas. *Nature* **448**, 684–687.

Jackson M. G., Hart S. R., Shimizu N. and Blusztajn J. S. (2009) The $^{87}Sr/^{86}Sr$ and $^{143}Nd/^{144}Nd$ disequilibrium between Polynesian hot spot lavas and the clinopyroxenes they host: evidence complementing isotopic disequilibrium in melt inclusions. *Geochem. Geophys. Geosyst.* **10**, Q03006.

Kasting J. F. (1993) Earth's early atmosphere. *Science* **259**, 920–926.

Kawabata H., Hanyu T., Chang Q., Kimura J.-I., Nichols A. R. L. and Tatsumi Y. (2011) The petrology and geochemistry of St. Helena alkali basalts: evaluation of the oceanic crust-recycling model for HIMU OIB. *J. Petrol.* **52**, 791–838.

Kelley K. A., Plank T., Ludden J. and Staudigel H. (2003) Composition of altered oceanic crust at ODP Sites 801 and 1149. *Geochem. Geophys. Geosyst.* **4**, 8910.

Keppler H. (1996) Constraints from partitioning experiments on the composition of subduction-zone fluids. *Nature* **380**, 237–240.

Kimura J.-I. and Nakano N. (2004) *Precise Lead Isotope Analysis using Multiple Collector-Inductively Coupled Plasma-Mass Spectrometry (MC-ICP-MS): Analytical Technique and Evaluation of Mass Fractionation During Pb Separation,* **vol. 23**. Shimane Univ Geosci. Rep..

Kogiso T., Tatsumi Y. and Nakano S. (1997a) Trace element transport during dehydration processes in the subducted oceanic crust: 1. Experiments and implications for the origin of oceanic island basalts. *Earth Planet. Sci. Lett.* **148**, 193–205.

Kogiso T., Tatsumi Y., Shimoda G. and Barsczus H. G. (1997b) High μ (HIMU) ocean island basalts in southern Polynesia: new

evidence for whole mantle scale recycling of subducted oceanic crust. *J. Geophys. Res.* **102**, 8085–8103.
Lassiter J. C., Blichert-Toft J., Hauri E. H. and Barsczus H. G. (2003) Isotope and trace element variations in lavas from Raivavae and Rapa, Cook-Austral islands: constraints on the nature of HIMU- and EM-mantle and the origin of mid-plate volcanism in French Polynesia. *Chem. Geol.* **202**, 115–138.
McKenzie D. (1989) Some remarks on the movement of small melt fractions in the mantle. *Earth Planet. Sci. Lett.* **95**, 53–72.
McKenzie D. and O'Nions R. K. (1983) Mantle reservoirs and ocean island basalts. *Nature* **301**, 229–231.
McNamara A. K., Garnero E. J. and Rost S. (2010) Tracking deep mantle reservoirs with ultra-low velocity zones. *Earth Planet. Sci. Lett.* **299**, 1–9.
Millet M.-A., Doucelance R., Schiano P., David K. and Bosq C. (2008) Mantle plume heterogeneity versus shallow-level interactions: a case study, the São Nicolau Island, Cape Verde archipelago. *J. Vol. Geotherm. Res.* **176**, 265–276.
Miyazaki T., Kanazawa N., Takahashi T., Hirahara Y., Vaglarov B. S., Chang Q., Kimura J.-I. and Tatsumi Y. (2009) Precise Pb isotope analysis of igneous rocks using fully-automated double spike thermal ionization mass spectrometry (FA-DS-TIMS). *JAMSTEC Rep. Res. Develop. Spec. Issue*, 73–80.
Nakagawa T. and Tackley P. J. (2005) The interaction between the post-perovskite phase change and a thermo-chemical boundary layer near the core-mantle boundary. *Earth Planet. Sci. Lett.* **238**, 204–216.
Nakamura K. and Kato Y. (2007) A new geochemical approach for constraining a marine redox condition of Early Archean. *Earth Planet. Sci. Lett.* **261**, 296–302.
Nakamura Y. and Tatsumoto M. (1988) Pb, Nd, and Sr isotopic evidence for a multicomponent source for rocks of Cook-Austral Islands and heterogeneities of mantle plumes. *Geochim. Cosmochim. Acta* **52**, 2909–2924.
Newsom H. E., White W. M., Jochum K. P. and Hofmann A. W. (1986) Siderophile and chalcophile element abundances in oceanic basalts, Pb isotope evolution and growth of the Earth's core. *Earth Planet. Sci. Lett.* **80**, 299–313.
Nielsen S. G. (2010) Potassium and uranium in the upper mantle controlled by Archean oceanic crust recycling. *Geology* **38**, 683–686.
Niu Y. and O'Hara M. J. (2003) Origin of ocean island basalts: a new perspective from petrology, geochemistry, and mineral physics considerations. *J. Geophys. Res.* **108**, 2209.
O'Connor J. M. and le Roex A. P. (1992) South Atlantic hot spot-plume systems: 1. Distribution of volcanism in time and space. *Earth Planet. Sci. Lett.* **113**, 343–364.
O'Connor J. M., Stoffers P., van den Bogaard P. and McWilliams M. (1999) First seamount age evidence for significantly slower African plate motion since 19 to 30 Ma. *Earth Planet. Sci. Lett.* **171**, 575–589.
Palacz Z. A. and Saunders A. D. (1986) Coupled trace-element and isotope enrichment in the Cook-Austral-Samoa Islands, Southwest Pacific. *Earth Planet. Sci. Lett.* **79**, 270–280.
Parai R., Mukhopadhyay S. and Lassiter J. C. (2009) New constraints on the HIMU mantle from neon and helium isotopic compositions of basalts from the Cook-Austral Islands. *Earth Planet. Sci. Lett.* **277**, 253–261.
Pilet S., Hernandez J., Sylvester P. and Poujol M. (2005) The metasomatic alternative for ocean island basalt chemical heterogeneity. *Earth Planet. Sci. Lett.* **236**, 148–166.
Pilet S., Baker M. B. and Stolper E. M. (2008) Metasomatized lithosphere and the origin of alkaline lavas. *Science* **320**, 916–919.
Reisberg L., Zindler A., Marcantonio F., White W., Wyman D. and Weaver B. (1993) Os isotope systematics in ocean island basalts. *Earth Planet. Sci. Lett.* **120**, 149–167.
Salters V. J. M. and White W. M. (1998) Hf isotope constraints on mantle evolution. *Chem. Geol.* **145**, 447–460.
Salters V. J. M. and Stracke A. (2004) Composition of the depleted mantle. *Geochem. Geophys. Geosyst.* **5**, Q05004.
Salters V. J. M., Mallick S., Hart S. R., Langmuir C. E. and Stracke A. (2011) Domains of depleted mantle: new evidence from hafnium and neodymium isotopes. *Geochem. Geophys. Geosyst.* **12**, Q08001.
Sato K., Tamura H., Kumagai H. and Hanyu T. (2005a) Application of K-Ar dating system to be performed by new noble gas mass spectrometry and its calibration from standard air analysis. Frontier Research on Earth Evolution 2, IFREE Report for 2003–2004.
Sato K., Tamura H., Nishio Y., Kumagai H. and Hanyu T. (2005b) Application of K-Ar dating performed by new technique of ultra low potassium analysis with new Zeeman atomic absorption photometry in clean room laboratory. Frontier Research on Earth Evolution 2, IFREE Report for 2003–2004.
Schiano P., Burton K. W., Dupré B., Birck J.-L., Guille G. and Allègre C. J. (2001) Correlated Os–Pb–Nd–Sr isotopes in the Austral-Cook chain basalts: the nature of mantle components in plume sources. *Earth Planet. Sci. Lett.* **186**, 527–537.
Shields G. and Veizer J. (2002) Precambrian marine carbonate isotope database: Version 1.1. *Geochem. Geophys. Geosyst.* **3**, 1–12.
Stacey J. S. and Kramers J. D. (1975) Approximation of terrestrial lead isotope evolution by a two-stage model. *Earth Planet. Sci. Lett.* **26**, 207–221.
Staudigel H., Plank T., White W. M. and Schmincke H. U. (1996) Geochemical fluxes during seafloor alteration of the basaltic upper crust: DSDP sites 417 and 418. In *Subduction: Top to Bottom, Geophys. Monogr. Ser* (eds. G. E. Bebout, D. W. Scholl, S. H. Kirby and J. P. Platt). AGU, Washington, D.C., pp. 19–38.
Steiger R. H. and Jäger E. (1977) Subcommission on geochronology: convention on the use of decay constants in geo- and cosmochronology. *Earth Planet. Sci. Lett.* **36**, 359–362.
Stracke A. (2012) Earth's heterogeneous mantle: a product of convection-driven interaction between crust and mantle. *Chem. Geol.* **330–331**, 274–299.
Stracke A. and Bourdon B. (2009) The importance of melt extraction for tracing mantle heterogeneity. *Geochim. Cosmochim. Acta* **73**, 218–238.
Stracke A., Bizimis M. and Salters V. J. M. (2003) Recycling oceanic crust: quantitative constraints. *Geochem. Geophys. Geosyst.* **4**, 8003.
Stracke A., Hofmann A. W. and Hart S. R. (2005) FOZO, HIMU, and the rest of the mantle zoo. *Geochem. Geophys. Geosyst.* **6**, Q05007.
Sun S.-S. (1980) Lead isotopic study of young volcanic rocks from mid-ocean ridges, ocean islands and island arcs. *Philos. Trans. R. Soc. Lond.* **A297**, 409–445.
Takahashi T., Hirahara Y., Miyazaki T., Vaglarov B. S., Chang Q., Kimura J.-I. and Tatsumi Y. (2009) Precise determination of Sr isotope ratios in igneous rock samples and application to micro-analysis of plagioclase phenocrysts. *JAMSTEC Rep. Res. Develop. Spec. Issue*, 59–64.
Tatsumi Y. (2005) The subduction factory: How it operates in the evolving Earth. *GSA Today* **15**, 4–11.
Tatsumoto M. (1978) Isotopic composition of lead in oceanic basalt and its implications for mantle evolution. *Earth Planet. Sci. Lett.* **38**, 63–87.
Thirlwall M. F. (1997) Pb isotopic and elemental evidence for OIB derivation from young HIMU mantle. *Chem. Geol.* **139**, 51–74.

Thirlwall M. F. (2000) Inter-laboratory and other errors in Pb isotope analyses investigated using a ^{207}Pb–^{206}Pb double spike. *Chem. Geol.* **163**, 299–322.

Vidal P. (1992) Mantle: More HIMU in the future? *Geochim. Cosmochim. Acta* **56**, 4295–4299.

Vidal P., Chauvel C. and Brousse R. (1984) Large mantle heterogeneity beneath French Polynesia. *Nature* **307**, 536–538.

Vollmer R. (1983) Earth degassing, mantle metasomatism, and isotopic evolution of the mantle. *Geology* **11**, 452–454.

Weaver B. (1991) The origin of ocean island basalt end-member compositions: trace element and isotopic constraints. *Earth Planet. Sci. Lett.* **104**, 381–397.

White W. M. and Hofmann A. W. (1982) Sr and Nd isotope geochemistry of oceanic basalts and mantle evolution. *Nature* **296**, 821–825.

White W., Hofmann A. W. and Puchelt H. (1987) Isotope geochemistry of Pacific mid-ocean ridge basalt. *J. Geophys. Res.* **92**, 4881–4893.

Willbold M. and Stracke A. (2006) Trace element composition of mantle end-members: implications for recycling of oceanic and upper and lower continental crust. *Geochem. Geophys. Geosyst.* **7**, Q04004.

Willbold M. and Stracke A. (2010) Formation of enriched mantle components by recycling of upper and lower continental crust. *Chem. Geol.* **276**, 188–197.

Woodhead J. D. (1996) Extreme HIMU in an oceanic setting: the geochemistry of Mangaia Island (Polynesia), and temporal evolution of the Cook—Austral hotspot. *J. Vol. Geotherm. Res.* **72**, 1–19.

Woodhead J. D. and Devey C. W. (1993) Geochemistry of the Pitcairn seamounts, I: source character and temporal trends. *Earth Planet. Sci. Lett.* **116**, 81–99.

Zindler A. and Hart S. (1986) Chemical geodynamics. *Annu. Rev. Earth Planet. Sci.* **14**, 493–571.

Associate editor: Andreas Stracke